Ph. D. Dissertation

Study on silicon-based microprobe electrode array with individual interconnects through substrate using silicon through-glass via

실리콘 관통 비아 전극을 이용한 개별 연결을 갖는 실리콘 기반 마이크로 프로브 전극 어레이에 대한 연구

2019 년 8 월

서울대학교 대학원

전기정보공학부

신 영 민

Study on silicon-based microprobe electrode array with individual interconnects through substrate using silicon through-glass via

지도교수 김 용 권

이 논문을 공학박사 학위논문으로 제출함

2019 년 8 월

서울대학교 대학원

전기정보공학부

신 영 민

신영민의 공학박사 학위논문을 인준함

2019 년 8 월

위 원 장 _____ **(인)**

부위원장 _____ **(인)**

위 원 _____ **(인)**

위 원 _____ **(인)**

위 원 _____ **(인)**

Abstract

This dissertation proposes a vertical out-of-plane microelectrode array (MEA) with an individual interconnect substrate, which uses a silicon through-glass via (TGV) with transparency properties. The MEA can be used for a wide variety of biological applications such as insertion in brain tissues for neural signal measurement. The problems of conventional MEAs that have been investigated in numerous studies include unwanted tissue damage caused by the insertion of an opaque microprobe electrode and the signal loss in the addressing line. To solve these problems, TGVs and microprobe electrode array were fabricated using low-resistance silicon (LRS) wafer and a glass reflow process. The MEA substrate made by the glass reflow process has high transparency, and thus, damage to the tissue can be minimized by inserting the microprobe electrode at the desired position. Furthermore, the glass substrate has excellent properties as an insulating film, thereby minimizing the signal loss between the silicon-via electrodes.

The diameter and height of the TGV structure are designed to be 80 μm and 250 μm, respectively. A deep reactive ion etching process is used as a fabrication method to etch silicon pillars with a diameter of 80 μm. After bonding the borosilicate glass wafer to the silicon substrate, the glass is reflowed at a temperature of 850 ℃. The transparency of the fabricated TGV structure was measured using a UV/Vis spectrophotometer. The measurement result showed a transparency of 60 % or more in the visible region. The resistance of single silicon via was measured to be 1.26 ± 0.041 Ω, and the cross-coupling capacitance was measured to be 0.23 ± 0.03 pF.

The height of the microprobe was designed to be greater than 90 μm for

insertion into the tissue, and the spacing between the microprobes was designed to be 210 μm to minimize chemical crosstalk between the microprobe electrodes. The microprobe structure is formed by combining the deep reactive ion etching and sulfur hexafluoride (SF_6) reactive ion etching processes using one-step photolithography and a single etching mask. The shape of the microprobe structure is obtained by the difference in the etching rate depending on the position of the silicon micropillar sidewall during the reactive ion etching process and depth of the first DRIE process.

To fabricate individual microprobe electrodes, a microprobe structure was exposed using a negative photoresist (DNR-L-300), and Cr and Au conductive layers of 200 Å and 2000 Å, respectively, were deposited. Following this, the electrode was patterned by a lift-off process, and a Parylene-C layer of 3000 Å was deposited on the electrode as an insulating film. Then, a self-alignment procedure was performed using a thick photoresist without a photolithography mask to expose the conductive layer only at the tip-end of the microprobe electrode. Each microprobe electrode was independently connected to the backside of the substrate through the silicon TGV.

To verify the electrochemical characteristics of the microprobe electrodes with individual interconnects, the steady-state limiting current through the redox reaction was measured for each electrode by the cyclic voltammetry (CV) method. The measured steady-state peak current of the microprobe electrode was compared with the theoretical calculation. Impedance measurements were performed on 16 electrodes, and the average impedance at 1 kHz was measured as 0.292 ± 0.156 MΩ. Then, an equivalent circuit analysis was conducted using the impedance modeling software (Zview, AMTEK Scientific instruments).

Following this, primary rat cortical neuron cells (DIV 7) were cultured on the fabricated microprobe electrodes and neural spike signals were successfully measured. The average signal-to-noise ratio (SNR) of the measured signal was 14.4. The fabricated electrode was then inserted into the hippocampal brain slice tissue of the rat and the experiment was conducted. Owing to the high transparency of the fabricated microprobe electrode, it was confirmed that tissue damage could be minimized by inserting the probe electrode at a desired position on the hippocampal tissue.

In conclusion, the proposed structure can measure signals with high SNRs and no chemical crosstalk by connecting the TGV and microprobe structures individually and it is possible to insert electrodes at the desired positions using a TGV structure with high transparency, thus minimizing damage to the target tissue. The proposed microprobe electrode is suitable to various bio application areas as it overcomes the limitations of the conventional MEA structure.

주요어 : Microprobe electrode array; Through glass silicon via (TGV); Glass reflow process; Self-alignment fabrication process; Transparency; Neural spike signal

학 번 : 2014-30299

Table of contents

List of tables

List of figures

Chapter 1. Introduction

1.1. Background

Since the first electrical signals associated with the brain were discovered by Richard Caton in 1875 [1], research has been actively conducted to uncover the secrets of electrical signals. Since then, the interest in science and medicine in relation to communication with the nervous system has increased steadily, and biomedical devices for measuring the nervous system have been actively studied [2-4]. Studies of the function and response of neurons play an important role in understanding the human mechanics. Particularly, studies on the exchange of electric signals between neurons in the brain, ear, eye, and spinal cord, which are important organs in the human body, are being actively studied [5-7]. The microprobe electrode array (MEA) makes it possible to measure the electrical signals between neurons [8]. The MEA device helps humans to better understand the neuron activities. Since the 1960s, MEAs have been studied as an important tool for measuring neural signals [9, 10]. In recent years, implantable MEAs provide easy access to the deep brain structure, increasing the signal-to-noise ratio (SNR) of the measured signal because of the short distance between the electrode and the neuron [11-13].

MEAs are used in many bio application areas such as neural signal measurement (cerebral cortex, retina, etc.), bio-potential measurements (ECG), drug delivery, and environmental sensors. This chapter presents a summary of the devices obtained by developing micromachining and biology techniques, such as the MEA, that can be used to measure neural signals [14-18].

1.1.1. Traditional neural probe

The first conventional implantable electrode was fabricated by sharpening metal wires in the 1950s [19]. Metal wire neural probes can be inserted *in vivo* causing minimal damage to the tissue during insertion. Because the neurons and electrodes are very close to each other during signal measurement, highly localized extracellular potentials can be measured [20].

Metal wire neural probes are made from wires of various materials, such as stainless steel, platinum, iridium, iridium oxide, gold, and tungsten, with diameters of approximately 100 μm [21-23]. To adjust the SNR and impedance of the measurement signal, an insulating film (Parylene-C, polyimide, Teflon) is deposited on the metal wire, except the wire end portion [24-26].

Figure 1-1 shows an SEM image of a conventional metal wire neural probe. The entire metal wire except its end was coated with Parylene-C.

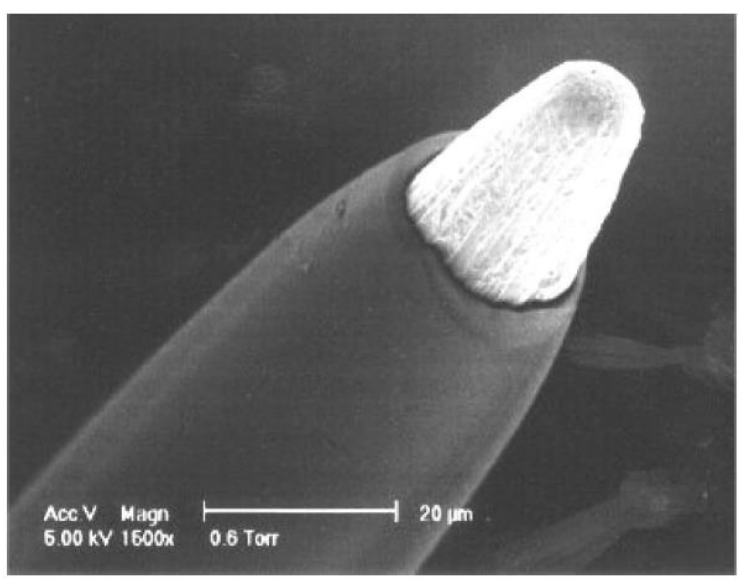

Figure 1-1. SEM image of metal wire coated with Parylene-C [19].

Later, the micro wire electrodes were glued adjacent to each other to form a multi-electrode array, which was developed as a device for measuring individual neural signals [27, 28]. Figure 1-2 shows images of a conventional metal wire electrode array.

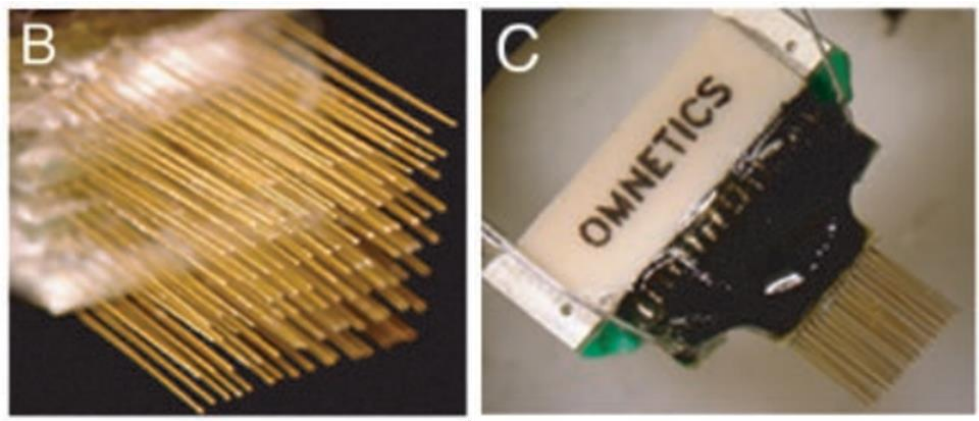

Figure 1-2. Conventional implantable metal wire electrode array [22].

To reduce the impedance of metal wire electrodes, research on the coating of metal wires with CNTs or an electrically conductive polymer was conducted for the first time in 2008 [29].

The micro wire electrode array has the advantage of easy access to the deep brain structure, but its disadvantage is that the metal wire can easily bend when inserted in the tissue. As the metal wires are manually glued, there is also a limitation for reducing the gap between electrodes. To solve this problem, many researchers have fabricated metal wire electrodes using iridium metal, which has high stiffness. However, iridium metal has the problem of increasing impedance, and it corrodes easily [30].

1.1.2. Silicon-based microprobes

Conventional metal wire electrodes have problems such as difficult miniaturization of the electrode spacing, non-uniformity of the electrode height, high impedance of the electrode, and bending during electrode insertion. These problems not only can cause tissue damage but also reduce the SNR of the measured signal [31]. To solve this problem, the electrode to be inserted should have biocompatibility and be very fine with a high stiffness.

To realize the properties of the electrodes mentioned above, research was conducted to fabricate silicon microprobe electrodes using the lithography process developed in 1959 and the rapidly developing silicon fabrication process technology [32]. The silicon fabrication process not only satisfies the conditions for fabricating ideal MEA electrodes but also can produce smaller MEA devices as the technology develops. In addition, since silicon-based microprobe electrodes and integrated circuit fabrication methods are compatible with each other, research is actively conducted to fabricate an MEA apparatus that combines the two structures. This electrode has the advantage of being able to simultaneously stimulate many neurons and measure their signals [33, 34].

1.1.2.1. The Michigan probes

One of the first silicon-based neural probes was developed at Michigan University during the 1970s [28]. The University of Michigan has been actively conducting research on various types of probe including single shaft, multi-shaft, and stacked-shaft structures [35-39]. The advantage of the Michigan probe structure is that it is advantageous for deep brain stimulation (DBS) because the recording and stimulation electrode is fabricated on a long shaft structure [40], as shown in Figure 1-3.

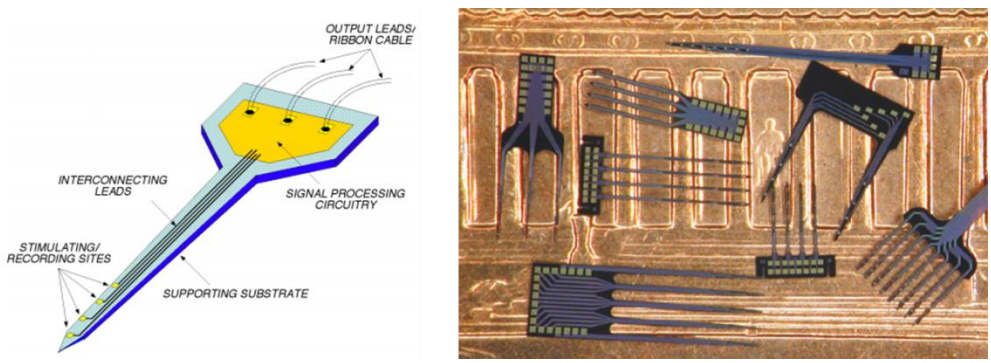

(a) (b)

Figure 1-3. Typical Michigan probe structure: (a) single-shaft, (b) multi-shaft [35].

Generally, the recording, stimulating, and signal transmission electrodes are made using iridium (Ir) or gold. To decrease the impedance value of the electrodes, their characteristics were improved using a conductive polymer and CNTs [41, 42], and electrical interconnects were formed on the surface to address each electrode individually. To minimize the signal loss caused along this addressing line, it is generally shielded using an insulating film. This structure is disadvantageous in that the noise of the measurement signal is increased owing to the parasitic capacitance caused by the insulating film deposited on the addressing line [43, 44].

To increase the density of the electrodes, M. D. Gingerich et al. fabricated a structure with 256 electrodes stacked in a 400 μm × 400 μm area using an additional silicon platform [45]. However, the silicon platform structure used in the 3-D stacked Michigan probes is mechanically unstable and fragile, which can seriously damage the tissue during insertion of the electrodes.

1.1.2.2. Utah array type neural probe

Another type of silicon-based MEA is the Utah array, shown in Figure 1-4. The Utah array type consists of needle-shaped electrodes arranged in a small area, and each electrode is electrically insulated [46-48].

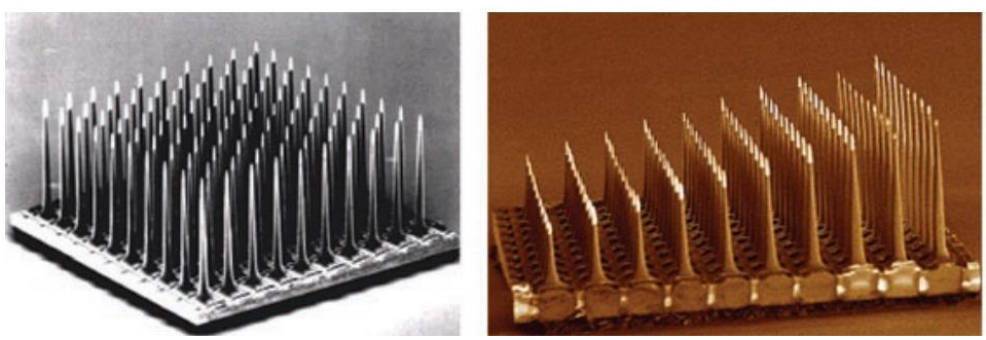

(a) (b)

Figure 1-4. Out of plane MEAs: (a) Utah electrode array, (b) Utah slanted electrode array [42].

The advantage of the Utah array is its mechanically stable structure and because the probe size is small, the insertion force can be reduced and the damage to the target tissue can be minimized [49, 50].

The generally Utah array structure is fabricated with a low-resistivity silicon wafer. A diamond saw creates the grid pattern on the silicon wafer and glass paste

is deposited to insulate each microprobe electrode [51]. After the silicon wafer is diced, the probe structure is fabricated by wet etching and reactive ion etching (RIE). A probe electrode is fabricated by depositing a conductive layer on the fabricated probe structure.

The Utah arrays have the disadvantage that it is difficult to fabricate probes with a height above 1.5 mm because of the silicon wafer thickness limitation. In addition, owing to the non-transparent characteristics of the substrate structure, it is impossible to insert the probe electrode at the desired which may cause damage to it [52], as shown in Figure 1-5.

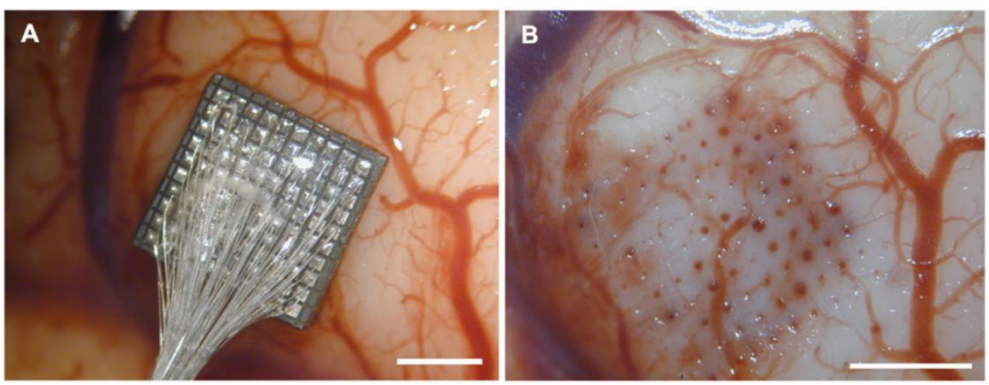

Figure 1-5. Tissue damage caused by opaque MEAs [52].

Kozai et al. reported that the SNR of neural signals was reduced by bleeding caused by opaque microprobe electrode insertion [53]. It was confirmed that the SNR value of the measured signal decreased when the bleeding duration after the microprobe electrode insertion was 15, 30, 60, 90, and 120 minutes, as shown in Figure 1-6. To overcome these disadvantages of the conventional MEA, a transparent structure capable of confirming the position where the electrode is inserted is required.

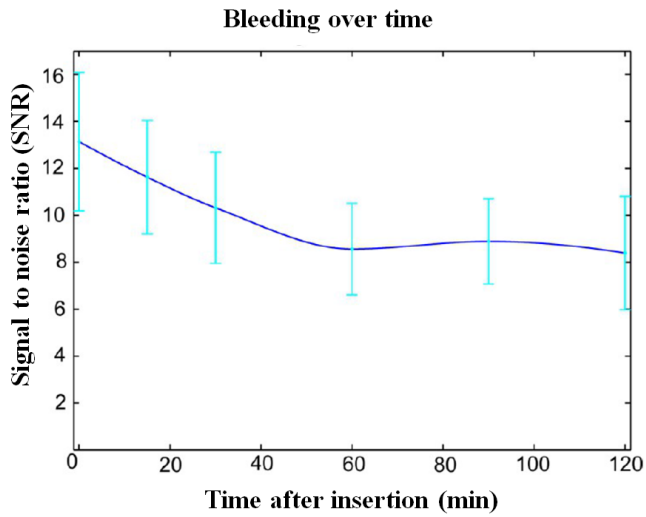

Figure 1-6. Decreased SNR value of measured neural signal due to bleeding [53].

1.2. Motivation and objectives

1.2.1. Motivation

Typical silicon-based MEAs are divided into in-plane (Michigan probe) and out-of-plane (Utah array) depending on the shaft shape. In-plane type MEAs can be made into a long shaft, which is advantageous for DBS experiments. However, to stack the shaft structure in the form of an array, an additional support structure is required with the disadvantage that it can be broken easily.

The signal is transmitted over an addressing line connected to the recording and stimulating electrodes of the long shaft. In general, the addressing line is shielded with an insulation layer to minimize the signal loss. In this case, as the addressing lines are long, a parasitic capacitance is generated between the metal lines, thereby causing a signal loss problem. It is known that the parasitic capacitance value has a disadvantage of increasing the noise of the signal and an additional compensation circuit is required to solve the problem [39].

In the case of the out-of-plane MEA, it is possible to increase the electrode density by fabricating it in a region narrower than the in-plane electrode. However, owing to the opaque property of the substrate, signal loss may be caused by unwanted damage to the target tissue [47]. This tissue damage reduces the SNR of the measured signal.

In this study, a new structure is proposed that can be applied to a wide variety of biological applications by solving the signal loss problem of the in-plane and out-of-plane MEAs caused by the addressing lines and the opaque structure.

1.2.2. Research objectives

This study aims to develop a silicon-based MEA using a silicon through-glass via (TGV) that can be applied to *in-vitro* applications. Previous studies had problems when measuring *in-vitro* signals because of the opaque property of the electrodes and the unwanted signal loss caused by the long addressing lines.

To overcome the unwanted signal loss, we aimed to fabricate a structure that minimizes signal loss in the measured signal transmission by using a silicon via made through a glass reflow process. In addition, as the electrode substrate made of reflowed glass has a transparency property, the electrode can be inserted at the desired position, thereby minimizing damage to the target tissue. The microprobe structure connected to the TGV is fabricated with the height and sharpness adjusted according to the target tissue to be measured.

The microprobe electrodes are fabricated using a combination of the anisotropic and isotropic etching processes. Through the deposition and etching processes of a conductive layer (Cr/Au) and an insulation layer (Parylene-C), the electrodes are formed at the end of the microprobe structure. Electrochemical experiments were performed to confirm the electrochemical properties of the fabricated microprobe electrode, and electrochemical crosstalk experiments were conducted to measure the crosstalk between microprobe electrodes.

In the *in-vitro* experimental part, neuron cells were cultured on the fabricated microprobe electrode, and a neural spike signal was measured to verify the use of the bio-application. The measured signal was analyzed to confirm that the action potential was successfully measured at the individual electrode and the SNR of the measured signal was high. In addition, the neural spike signal was successfully

measured by inserting the microprobe electrode into a hippocampal brain slice and it was confirmed that the tissue could be observed through the transparent electrode.

1.3. Contents and organization

This study includes two main contents. The first one focuses on the combination of the TGV and microprobe electrode structures. In the second one, electrochemical and *in-vitro* experiments using microprobe electrodes are performed and analyzed.

The document is organized as follows. First, the structure of the TGV and microprobe electrode is introduced, and the design process is explained.

Next, the fabrication process of the MEA is introduced with explanation of the combination of multiple deep reactive ion etching (DRIE) and RIE processes.

Next, the signal measurement method of culturing rat cortical neuron cells in the MEA and the measurement results are described. Then, we analyze the measured neural spike train signal using a custom algorithm. After that, the electrode insertion experiment using the hippocampal brain slice is described and the experimental results are presented. Finally, the results of the analysis based on the measured signal are discussed.

Chapter 2. Design of MEA with TGV structure

2.1. Introduction

Over the past several decades, as the micromachining technology has evolved rapidly, technologies for fabricating three-dimensional structures on a micrometer scale have been continuously developed and reported. One of these structures is the microprobe electrode, which with its sharpened feature has a wide variety of applications, such as in tactile displays, field emission probes, super hydrophobic surfaces, and biological studies [54-58].

In biological applications, microprobe electrodes are generally used as neural probes. It is an advantageous structure that easily penetrates the dead cell layer of the target tissue and measures the electrical signal of the internal organism using its sharpened characteristic. In addition, as the apex radius of the microprobe electrode is very small, it has the advantage that the target tissue is not seriously damaged during the experiment [59, 60].

In addition, research on microprobe electrodes as photosynthetic electrochemical fuel cells that directly extract the electrons generated by the photosynthesis reaction in chloroplasts in algae cells has been reported. They are more efficient than other photosynthetic electrochemical fuel cells because the conductive layer of the microprobe electrode is exposed only at the tip-end [16].

Generally, the sharpness and aspect ratio of the tip-end are very important specifications, depending on the microprobe application. To control these specifications, silicon is a highly suitable material owing to the well-established

etching techniques. In addition, its mechanical stability and high stiffness are considered to be advantages for fabricating various three-dimensional structures. The shape of the silicon microprobe is determined according to various fabrication methods. To realize the vertical shape of the microprobe with a high aspect ratio, bulk micromachining and surface micromachining techniques, which are basic processes in micromachining technology, are generally used [61, 62].

One of the best-known and simpler silicon microprobe fabrication methods is wet etching, which enables different etching rates depending on the crystal orientation of silicon [63]. This method is efficient because only one etching process is required to fabricate the microprobe structure. However, as the etching rate is fixed according to the crystal orientation, the microprobe is formed into a pyramidal shape and is not suitable for insertion into tissues. To solve this problem, a fabrication method combining dry wet etching processes has been reported.

The combination of anisotropic and isotropic etching makes it possible to easily fabricate various types of high aspect ratio silicon structures. DRIE and RIE are typical dry etching methods and have anisotropic and isotropic etching characteristics, respectively. J. G. Ha et al. described the combination of DRIE and RIE processes to control the silicon needle aspect ratio and apex radius according to the pattern size and spacing of the silicon pillars [64]. However, a problem with this fabrication method is that microprobe structures are not fabricated when the spacing between the patterns increases. To overcome this problem, our previous study reported that a wide gap in the microprobe structure can be obtained using multiple DRIE and RIE processes [65].

To sense electrical signals in a specific area within a living tissue, the

conductive layer of the microprobe electrode must be in the tip-end area and the remaining area should be electrically isolated. T. Wang et al. proposed an electrode structure optimized for neural recording by analyzing the change in impedance value according to the area of the conductive layer exposed at the tip-end [66]. In many previous studies, the fabrication of the conductive part of microprobe structure has been introduced [17].

In the neural probe applications reported in previous studies, it was difficult to insert the microprobe electrodes at the desired location owing to the opaque substrate properties. Because of this problem, tissue damage may occur when the electrode is inserted. It has been reported that tissue damage causes inflammation at the area of insertion and noise in the measured signals [47].

In addition, the addressing line for transmitting the measured signal to the outside is one of the important factors of signal loss. The well-known MEA structure is fabricated with individual electrodes by connecting an addressing line to each microprobe electrode. The insulation layer is used to electrically shield the addressing line to minimize noise. However, this structure is known to cause undesired parasitic capacitance owing to the insulating layer deposited on the addressing line when the tissue or cell is placed on the electrode during a biological experiment [67, 68].

To solve these problems and based on our previous work, this chapter presents the design of a MEA using a TGV structure, a fabrication process of a conductive microprobe array, and a TGV structure [69, 70]. To realize a transparent structure and separate the addressing lines, a low-resistance p-type wafer is subjected to a DRIE step to form a silicon pillar and then the silicon wafer and the glass wafer are

bonded through a low-vacuum anodic bonding. A glass reflow step is performed to fabricate the TGV structure.

2.2. Design of proposed structure

2.2.1. Design of combined microprobe and TGV electrode

Figure 2-1 shows a schematic view of the proposed device. The device consists of a microprobe electrode part and a TGV part. First, the TGV structure is fabricated using a glass reflow process. The TGV structure is designed to fill the gap between the silicon vias with glass, which is an insulating material, so as to minimize the loss of the individually measured signals.

After that, the silicon microprobe structure is formed on the TGV structure and individually interconnected to the backside of the substrate. After the conductive layer is deposited on the microprobe structure, a mask-less self-alignment process is performed to expose the electrode only at the tip-end to minimize signal loss.

Unlike the planar electrode structure, the out-of-plane microprobe electrode has a three-dimensional recording surface around the tip-end of the exposed electrode. It has the advantage of being less influenced by the orientation of neurons or the measurement target and other factors [71]. Further, the microprobe electrode can be fabricated as an array structure, and the reaction can be individually measured at each position of the target. The vertical silicon vias through the substrate can shorten the transmission distance, thus reducing the signal noise, and can be integrated in CMOS chip applications [72].

Except for the silicon vias and microprobe electrodes, the fabricated microprobe electrode structure consists of a transparent glass substrate fabricated by a glass reflow process. As a result of these structural features, the fabricated

microprobe electrode has high transparency. Because of this feature, it is possible to insert the proposed microprobe electrode at the desired position of the tissue during a biological experiment, thereby minimizing damage to the tissue.

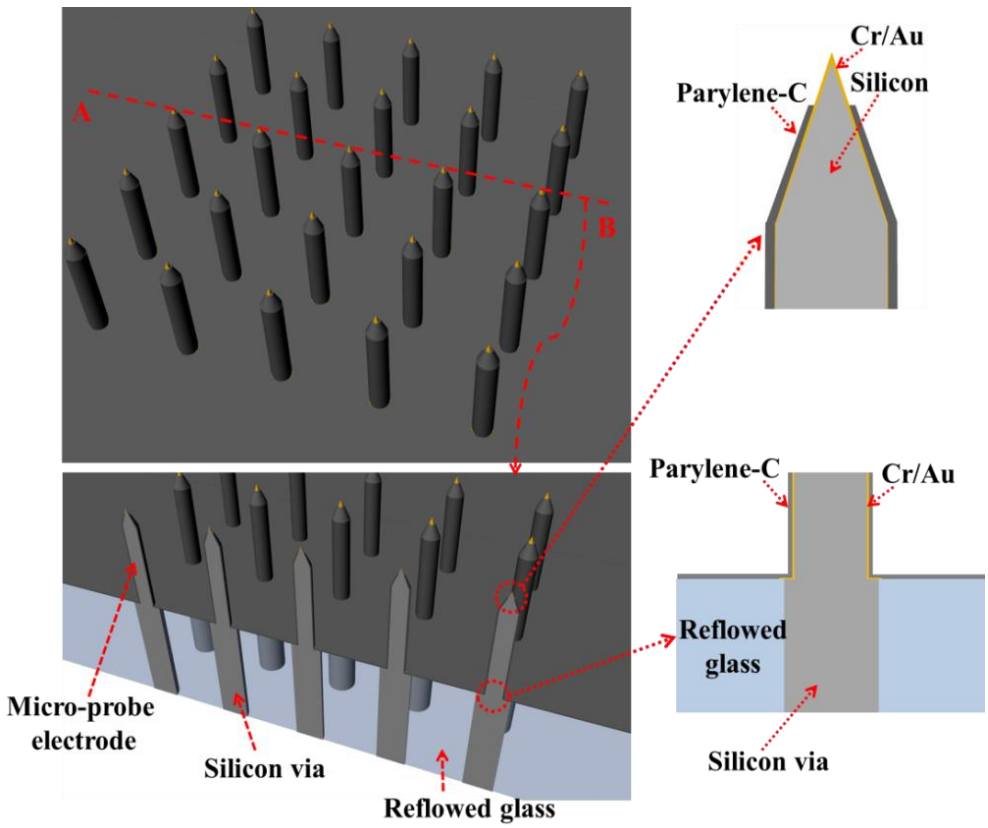

Figure 2-1. Proposed structure of microprobe electrode array (MEA).

2.2.2. Design of conductive microprobe

The design parameters of the proposed MEA are shown in Figure 2-2. The structure of the MEA proposed in this study was designed as a 4 × 4 electrode array. The pitch of each electrode is designed to be 210 μm, thus minimizing the electrochemical crosstalk and enabling the microprobe electrode to efficiently measure signals over a wide area. In addition, as each microprobe electrode is inserted and measured inside the tissue, the height of the electrode is designed to be 90 μm or more.

The MEA is designed to minimize signal loss by exposing the conductive layer of the tip-end portion to obtain a high SNR ratio of the measured signal. The localized electrode exposure of the microprobe proceeds through a self-alignment process using a thick photoresist without an additional photolithography step on the electrode on which the insulating layer is deposited.

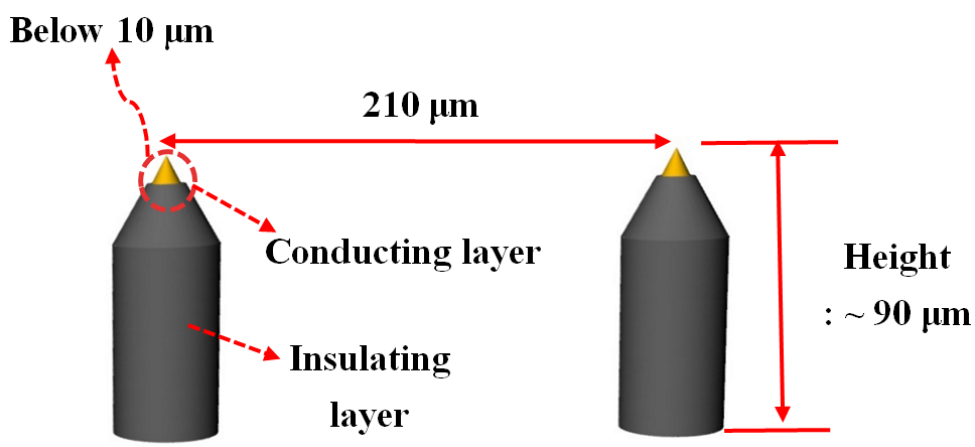

Figure 2-2. Design parameters of MEA microtip.

2.2.3. Design of TGV structure

The application of the MEA proposed in this study aims at minimizing the damage of the target tissue and measuring the neural signal. To achieve this, the microprobe electrode is designed to have a transparent structure so that the electrode can be inserted at a desired position of the tissue. To ensure the transparency of the silicon via structure, glass is filled between the silicon via electrodes without any gaps so that the signal loss between the silicon vias is minimized and the transparency is ensured.

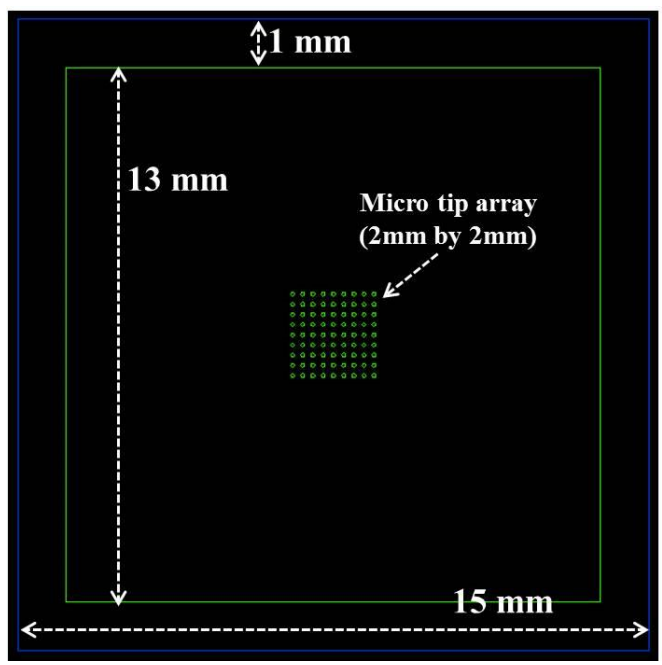

Figure 2-3. Mask layout of MEA

The total chip size of the microprobe electrode structure was designed to be 15 mm × 15 mm. The size of the microprobe structure was 11 mm × 11 mm and the size of the TGV structure was designed as 13 mm × 13 mm. This is shown in Figure 2-3. Silicon vias are designed to have a thickness of 250 μm and a diameter

of 80 μm for the stability of the TGV structure. Moreover, as the silicon vias must be individually connected to the microprobe electrodes, the pitch of the silicon vias is designed to be of 210 μm, which is equal to the pitch of the microprobe electrodes.

Chapter 3. Fabrication of MEA structure combined with TGV structure.

3.1. Introduction

This chapter describes the fabrication process and results of the microprobe electrode array combined with the TGV structure. The fabrication process is divided into the TGV fabrication process and the MEA fabrication process.

We describe the fabrication process and results of TGV structure after low-vacuum anodic bonding of the glass wafer and silicon pillar structure. Then, we describe the fabrication process and results of the microprobe using multiple DRIE and RIE processes and also describe the changes in the sharpness and aspect ratio of the microprobe structure by controlling process parameters. In addition, the self-alignment fabrication process for exposing the conductive layer only at the tip-end is presented.

Finally, the results of the transparency experiment of the fabricated MEA are presented.

3.1.1. Basic fabrication process

Figure 3-1 shows the fabrication process of the TGV structure. First, a silicon pillar is fabricated through a vertical etching process with a silicon substrate as the base. After the borosilicate glass wafer is bonded to the substrate with the silicon pillar, a vacuum anodic bonding is performed and then a glass reflow process is performed at 850 ℃ for 3 h. Then, the TGV structure is fabricated by removing the unnecessary glass part through a chemical mechanical polishing (CMP) process.

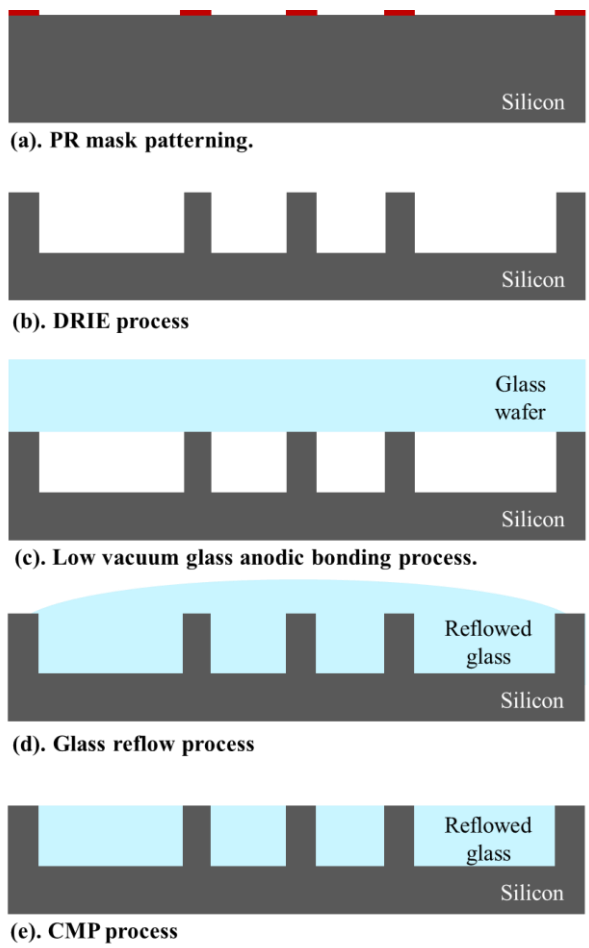

Figure 3-1. Fabrication process of TGV structure.

The microprobe electrodes are fabricated by depositing a conductive layer on a silicon-based microprobe structure, depositing an insulating layer over the probe structure, and etching the insulating layer only at the tip-end. Figure 3-2 shows the process of fabrication of the MEA. First, the silicon substrate is vertically etched using an anisotropic process. The silicon pillars are fabricated in the form of a wine glass structure using the property that the isotropic etching process using SF_6 gas has a high etching rate at the bottom of the silicon pillar. The second anisotropic process then increases the height of the wineglass structure. The second isotropic process then completes the probe structure by etching the thin portion of the wineglass structure. A Cr/Au layer is deposited as a conductive layer on the fabricated microprobe structure, and a Parylene-C insulation layer is deposited. Then, the photoresist is coated on the probe structure, and an isotropic process using O_2 gas is performed to expose the electrode at the tip of the probe.

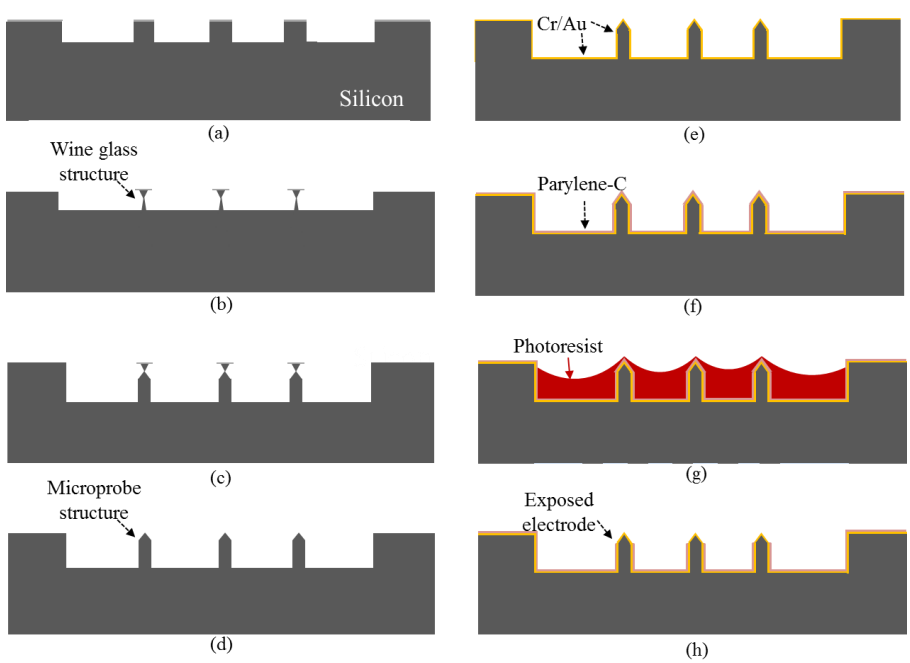

Figure 3-2. Fabrication process of microprobe electrode structure.

3.2. Microprobe formation mechanism

A schematic view of the mechanism by which the microprobe structure is formed is shown is Figure 3-3. First, a silicon substrate is vertically etched using an anisotropic etching process and an upper mask to fabricate a cylindrical silicon structure, as shown in Figure 3-3(a). During the isotropic process using SF_6 gas, the silicon pillar is converted to the wineglass form, as shown in Figure 3-3(b). This is because the etching rate depends on the position of the sidewall of the silicon pillar during the isotropic etching process.

The reason why the etching rate is changed can be determined by investigating the mechanism of the RIE process. The RIE used in this process is a combination of ion-enhanced and chemical etching processes. The ion-enhanced etching is anisotropic, with the ion distribution or angle depending on the applied bias voltage. The chemical etching is affected by neutral radicals depending on the temperature and is characterized by isotropic etching and undercutting of the structure. In the RIE process using a silicon pillar, the incident ions are masked by the silicon pillar structure to reduce the etching rate and cause an undercut phenomenon at the bottom of the structure. As a result, the pillar structure is etched into a negative profile shape and transformed into a wine glass form [73]. Then, an anisotropic etching process is carried out to increase the height while maintaining the shape of the wine glass, as shown in Figure 3-3(c). Finally, the RIE process is carried out once more to convert the wineglass structure into a microprobe structure, as shown in Figure 3-3(d). By using this process, a wide pitch cylindrical pillar structure can be fabricated with a microprobe structure of various heights.

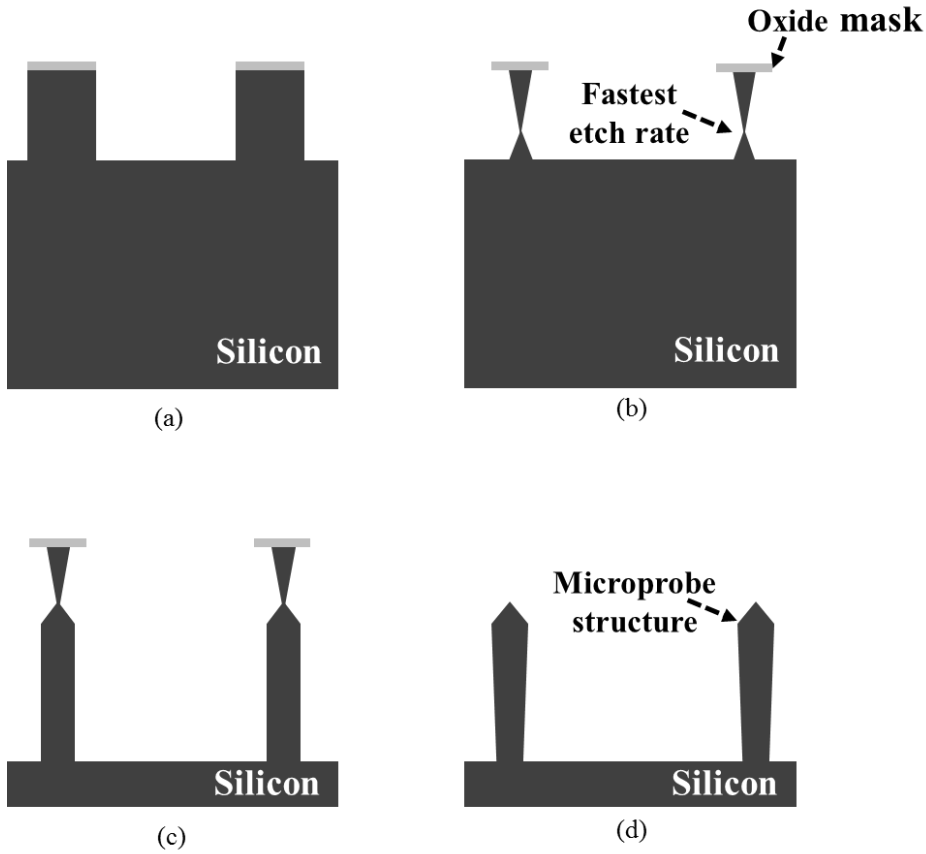

Figure 3-3. Schematic view of the microtip formation mechanism.

3.3. Detailed fabrication process

The proposed fabrication method is shown in Figure 3-4. First, cleaning is carried out for 20 min using a solution prepared by Piranha solution (4:1 mixture of 98% H_2SO_4 and 30% H_2O_2) with a low resistance (0.01–0.03 Ω·cm) silicon p-type wafer having a thickness of 525 μm. Then, a 1 μm SiO2 layer is deposited on a silicon wafer by plasma-enhanced chemical vapor deposition (PECVD). Then, a photolithography (MA-6, Karl Suss) process is conducted using an AZ4330 positive photoresist and patterning is performed. After patterning, SiO_2 is patterned using the photoresist as a mask.

Then, the DRIE process is performed to fabricate a silicon pillar structure having a height of 280 μm. The DRIE process conditions used in this study are the same as those presented in Table 3-1. After forming the silicon pillar, the photoresist on SiO_2 is removed using an oxygen (O_2) plasma system (V15-G, Plasma-finish). The remaining SiO_2 is removed using a 49% concentrated hydrofluoric acid (HF) solution. After that, borosilicate glass wafer is washed with Piranha solution (4:1 mixture of 98% H_2SO_4 and 30% H_2O_2). Using a RIE etcher (RIE 80 plus, Oxford Instruments), a glass treatment is performed using the fabrication conditions specified in Table 3-1. The reason for this glass treatment is to prevent crystallization of the glass during the glass reflow process [74].

Thereafter, the glass wafer is anodically bonded to the silicon wafer at a low vacuum (10^{-3} Torr). After the anodic bonding process, the reflow process is performed at 850 ℃ for 3 h in the furnace, filling the space between the silicon pillars. Through this glass reflow process, the silicon pillar structure is connected to the microprobe electrode as a TGV structure to transmit the signal. After the reflow

process, CMP is performed to remove unnecessary glass parts. First, the back side of the wafer is polished, and the front side of the wafer is also polished to adjust the wafer thickness to 450 μm. After that, the wafer is cleaned and a PECVD process is performed on the back side of the wafer after the polishing process, thereby depositing a SiO_2 layer at a thickness of 1.5 μm. After SiO2 layer deposition, patterning is carried out using an AZ 4330 photoresist. Patterning of the SiO_2 layer is performed using the patterned photoresist as a mask.

Multi-DRIE and RIE processes, consisting of two DRIE and two RIE processes, are performed to fabricate the microprobe. First, the DRIE process, which is an anisotropic etching process, is performed to fabricate a cylindrical silicon pillar structure having a height of 50 μm. The process conditions used in the DRIE process are presented in Table 3-1. Then, the isotropic etching process, an RIE process in an inductively coupled plasma (ICP) etcher (SLR-880-10R-B, Oerlikon), is performed to etch the cylindrical silicon pillar structure into a wineglass shape to determine the cone shape of the microprobe. The process conditions used in the RIE are listed in Table 3-1. Then, the second DRIE process is performed to increase the height of the wineglass to determine the height of the microprobe. The fabrication is performed so that the reflowed glass surface is exposed at the same time when the microprobe structure is completed through the RIE process. At this time, the fabricated microprobe structure is connected to the TGV structure to form an individual electrode structure. The second RIE process is used to etch the wineglass to complete the process in the form of a microprobe having a height of 90 μm. Then, to use a lift-off process, which is a process for forming a conductive layer on each microprobe structure, a pattern is formed so

that electrodes can be deposited only on the microprobe structure using a negative photoresist (DNR-L300, Dongjin). After patterning, Cr/Au (200/2000 Å) is deposited on the microprobe structure as a conductive layer using metal sputtering (SPS4150, Ultech). Then, a lift-off process is performed using an acetone solution so that a conductive layer remains only in the microprobe structure.

To proceed with the chip level process, the wafer is subjected to a dicing process to cut the chips into a single size of 15 mm × 15 mm. For electrical isolation, the insulating film, Parylene-C, is deposited on the surface of the microprobe electrode to a thickness of 3000 Å. After Parylene-C deposition, the entire microprobe structure is spin-coated using a viscous photoresist (AZ4620, Clariant) to expose the conductive layer of the tip of the probe. The spin coating process is carried out according to the conditions in Table 3-1. After the spin coating process, hard bake is carried out on a hot plate at 85 ℃ for 2 h. The hard baking temperature is low because a bubble is generated in the photoresist coated on the microprobe structure when the hot plate temperature is high. After baking, the temperature of the hotplate is decreased at 1 ℃/min to room temperature to prevent cracking of the photoresist owing to the rapid temperature change. A total of two spin coating operations are performed under the same fabrication process conditions. Whenever spin coating is performed, the photoresist is coated to a thickness of 50 μm. When the coating process is completed twice, it is coated in a total thickness of 100 μm, and the microprobe cone portion is coated with a thinner photoresist than the other portions. As the photoresist of the cone portion is coated very thinly compared to the other portions, an RIE process for etching the photoresist and Parylene-C is performed. The isotropic RIE process was performed

with an RF power of 200 W at an O_2 gas flow rate of 100 sccm and 5 sccm of Ar under 100 mTorr of pressure. In the RIE process, the etch rate is similar to that of Parylene-C because of the low selectivity of the coated photoresist. First, the thin photoresist of the cone portion is etched, and then the exposed Parylene-C layer is etched to expose the conductive layer at the tip-end. The RIE process condition is summarized in Table 3-1. The remaining photoresist is removed using AZ700 photoresist remover (Clariant) heated to 120 ℃. A lift-off process is performed to wire-bond the backside via of the fabricated MEA. The wire bonding pad is patterned using DNR-L300 photoresist and the lift-off process is performed by depositing Cr/Au (200/2000 Å). Table 3-1 presents the sequence of detailed fabrication processes.

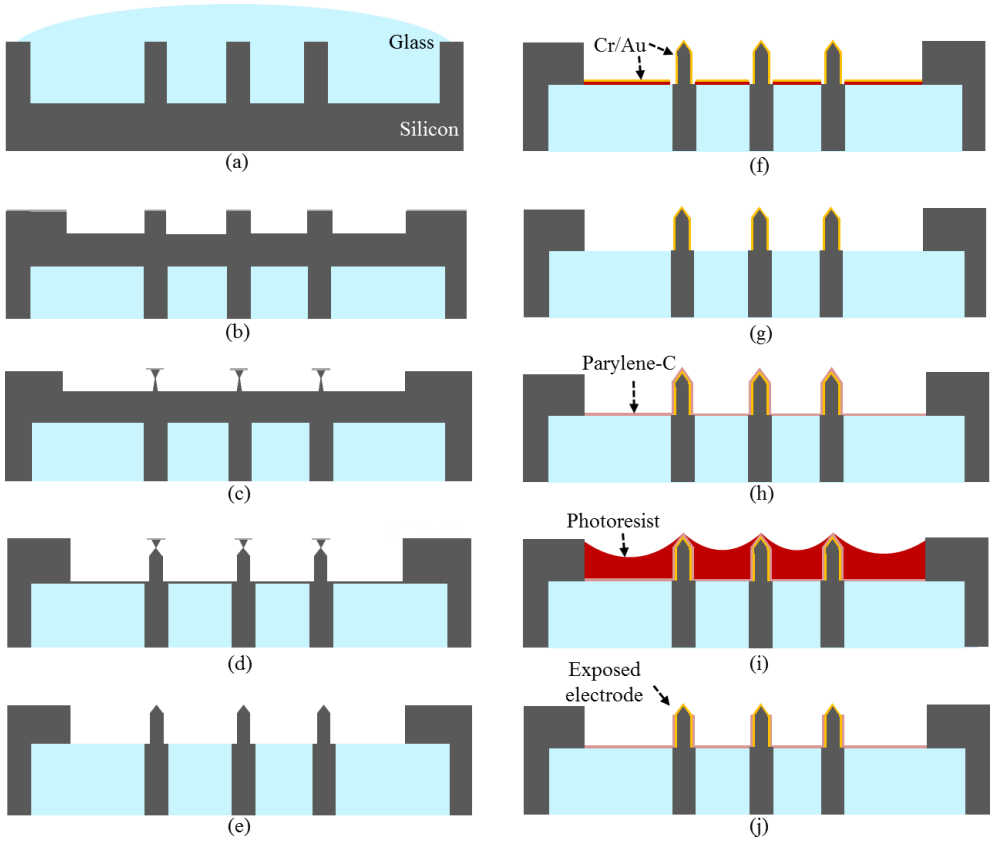

Figure 3-4. Fabrication process: (a) DRIE and glass reflow process to form TGV structures, (b) CMP process and silicon pillar patterning with DRIE on the backside of the substrate, (c) isotropic etching of the silicon pillar using RIE process, (d) anisotropic etching of the silicon substrate with DRIE process, (e) isotropic etching of the silicon pillar using RIE process to form sharp microtip end, (f) patterning of the photoresist and sputtering of Cr/Au conductive layer, (g) lift-off process to pattern conductive layer on the microprobe structure, (h) deposition of insulation layer using Parylene-C, (i) photoresist spin coating, (j) Parylene-C etching and photoresist removal.

Table 3-1. Sequence of detailed fabrication processes.

Step	Fabrication	Machine	Detailed condition
10	SPM cleaning	Wet station	Piranha solution, 10 min
20	SiO_2 deposition	P-5000 CVD	1 μm thickness
30	Photolithography	MA6-3	AZ4330, 3 μm thickness
40	SiO_2 etching	P-5000 Etch	20% over etching
50	PR removal	Asher	10 min
60	PR removal	Wet station	Piranha solution, 10 min
70	Deep silicon etching	DRIE etcher	250 μm depth
80	Glass treatment	Oxford 80+ etcher	Cl_2: 50 sccm, pressure: 55 mTorr, 3 min
90	Anodic bonding	EVG wafer bonder	1 mTorr, low pressure bonding
100	Glass reflow	Minifurnace	850 ˚C, 3 h
110	CMP		Wafer thickness 450 μm
120	Wafer cleaning	Wet station	Piranha solution, 10 min
130	SiO_2 deposition	P-5000 CVD	1 μm thickness
140	Photolithography	MA6-3	AZ 4330, 3 μm
150	SiO_2 etching	P-5000 Etch	20% over etching
160	Dicing	DAD 522	150 W, 20 min
170	DRIE	DRIE etcher	50 μm depth
180	RIE	DRIE etcher	Only $SF_{6:}$ 100 sccm, 6 min

190	DRIE	DRIE etcher	Etch until the glass surface is partially exposed.
200	RIE	DRIE etcher	Etch until the glass surface is completely exposed.
210	Sample cleaning	Wet station	Piranha solution, 10 min
220	Photolithography	MA6-3	DNR-L300, 3 μm
230	Metal deposition	Au sputter	Cr/Au (200/2000 Å)
240	Lift-off process	Sonicator	Acetone (3 min)
250	Parylene-C coating		3000 Å thickness
260	PR spin coating	Spin coater	AZ 4620, 40 μm
270	PR spin coating	Spin coater	AZ 4620, 40 μm
280	Parylene-C etching	Oxford 80+ etcher	100 sccm O_2, 5 sccm Ar, 7 min
290	PR removal	Wet station	AZ 700 (3 min)
300	Metal deposition	Au sputter	Cr/Au (200/2000 Å)
310	Photolithography	MA6-3	AZ4330, 3 μm
320	Metal etch	Wet station	Cr/Au wet etch

3.4. Fabrication results

In this section, we will discuss the fabrication results of the MEA structure. Figure 3-5 shows the fabrication result of the TGV structure. It was confirmed that the reflowed glass between the silicon pillars was filled without any gap. The silicon pillars are isolated from each other with the glass interposer, which are silicon TGVs for the individual interconnection of the microprobe electrodes. Figure 3-5(a) presents an optical microscope image, and it is confirmed that the reflowed glass fills around the pillar without crystallization. Figure 3-5(b) shows the difference in height between the silicon via surface and the reflowed glass surface after the CMP process using a laser profiler (VF-7510, KEYENCE). As a measurement result, it was confirmed that the reflowed glass surface was 0.94 ± 0.08 μm lower than the silicon via surface. Figure 3-5(c) is a SEM image of the fabricated TGV structure. Figure 3-5(d) is a cross-sectional SEM image of the fabricated TGV structure and confirmed that the glass around the silicon via was filled with reflowed glass.

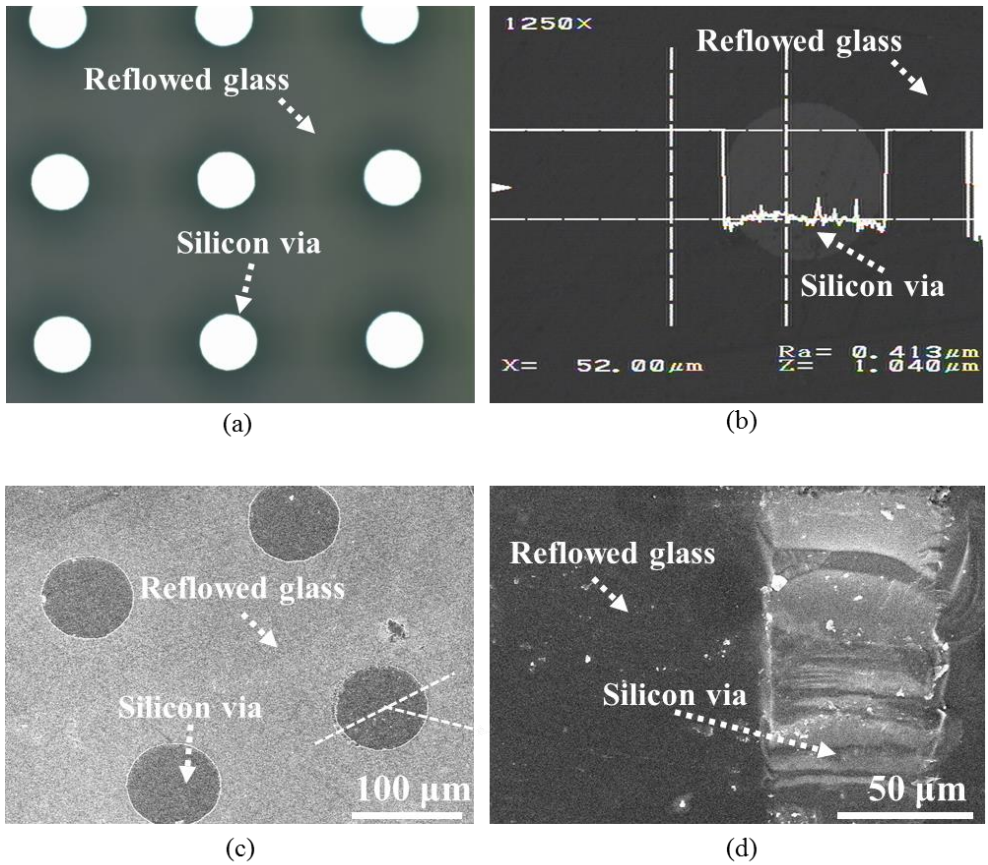

Figure 3-5. Fabrication results of silicon TGVs: (a) optical microscope image of the fabricated silicon TGVs, (b) surface profile measured after CMP process, (c) SEM image of silicon TGVs, (d) cross-sectional SEM image of silicon TGV.

To measure the electrical resistance of the fabricated silicon TGV, the Cr/Au (200/2000 Å) layer was patterned on the TGVs to connect two adjacent vias and subsequently annealed at 350 ℃ to reduce the contact resistance. Therefore, a pair of silicon TGVs is serially connected through the patterned Cr/Au layer and the resistance was measured at the probe station (MST 8000C, MSTECH). The resistivity of the original p-type low-resistance silicon (LRS) wafer was measured to be 0.017 ± 0.07 Ω·cm. The length and diameter of the measured silicon via are

250 μm and 80 μm, respectively. The resistance of single silicon via was measured to be 1.26 ± 0.041 Ω, which is less than the calculated value using the resistivity of the original LRS wafer.

The fabricated microprobe structure in this study was fabricated by multi-DRIE process and RIE process. The etching characteristics that change the height and sharpness of the fabricated microprobe structure according to fabrication process parameters will be discussed. Figure 3-6 is an SEM image of a microprobe produced by the first DRIE depth change. The conical sharpness and conical height of the fabricated microprobe structure change as the first DRIE depth is etched to 50, 100, and 150 μm, respectively. Figure 3-7 shows the measured conical tip height and tip-end angle increasing with the first DRIE depth. The smaller the first DRIE depth is, the better the conical sharpness of the fabricated microprobe structure and the higher the conical height. The tapered tip-end angle denoted by the inset in Figure 3-7 was measured at 13°, 28°, and 34°, with first DRIE depth of 50, 100, and 150 um, respectively. As the cone sharpness of the microprobe structure increases, the insertion force required to insert it into the tissue to be measured during the biological experiment is reduced, thus minimizing the tissue damage [18].

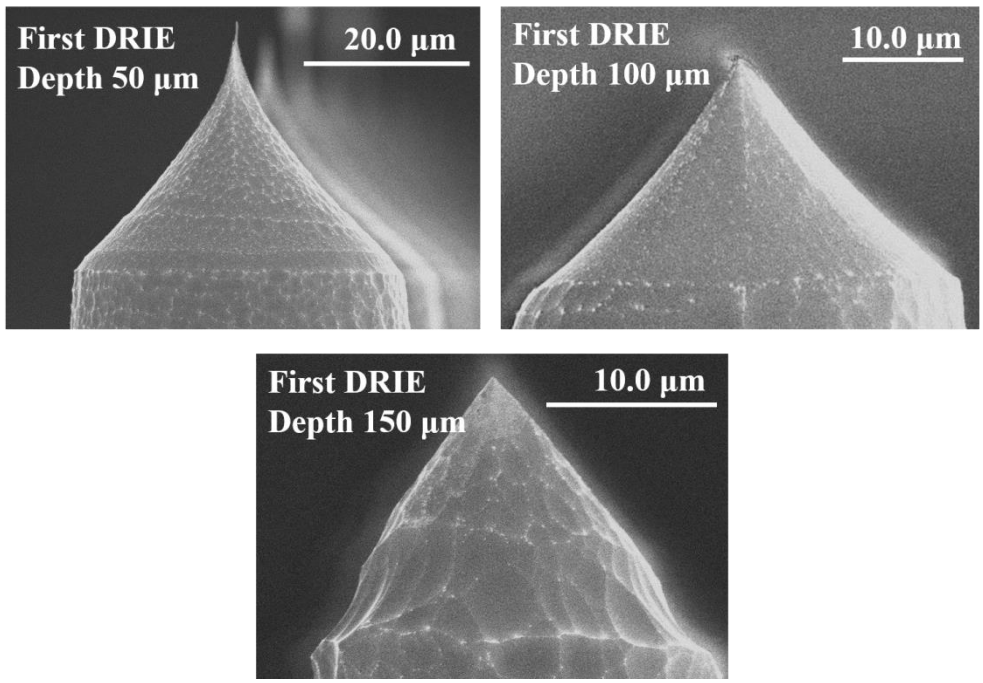

Figure 3-6 Fabrication results of microprobe structure according to first DRIE depth.

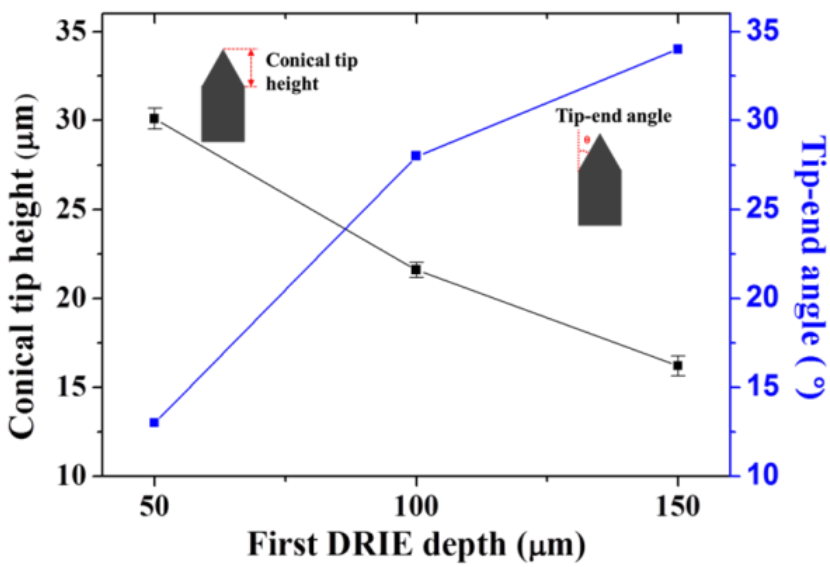

Figure 3-7. Measured conical probe height and tip-end angle with increasing first DRIE depth.

Figure 3-8 presents the fabrication result of coating the viscous photoresist to expose the conductive layer of the probe tip after depositing the Cr/Au layer and the Parylene-C insulation layer on the microprobe. As can be seen in Figure 3-8(a), the photoresist is coated on the entire structure, and the tip-end portion is coated with a thin layer of photoresist compared to the other portions. Figure 3-8(c) is the fabrication result of etching the photoresist and Parylene-C thinly coated on the tip-end by the RIE process. The thin layers of photoresist and Parylene-C are etched through the RIE process to expose the conductive layer. Figure 3-8(b) is a SEM image of the MEA after the remaining photoresist is removed. It can be seen that the microprobe is successfully formed on the TGV structure and the microprobe electrode is electrically insulated by the reflowed glass.

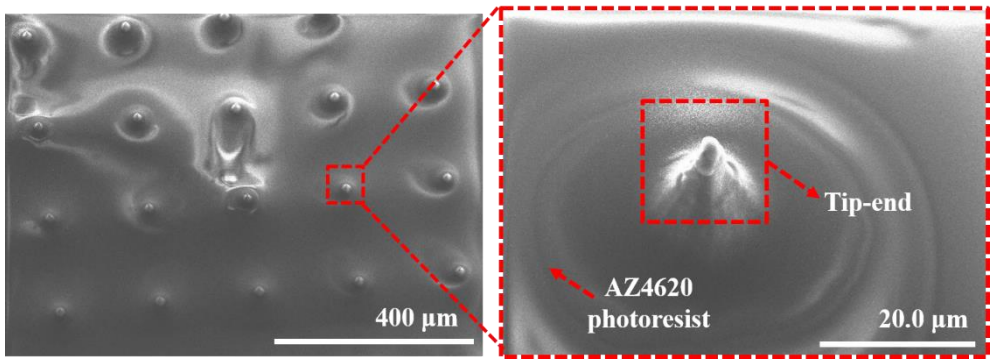

(a)

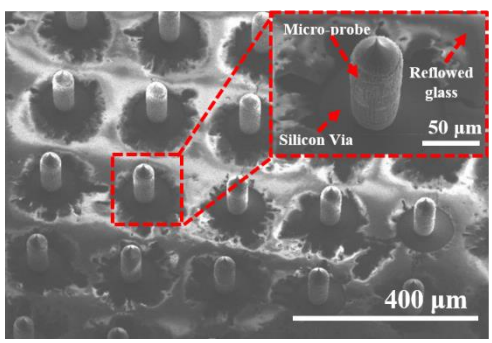

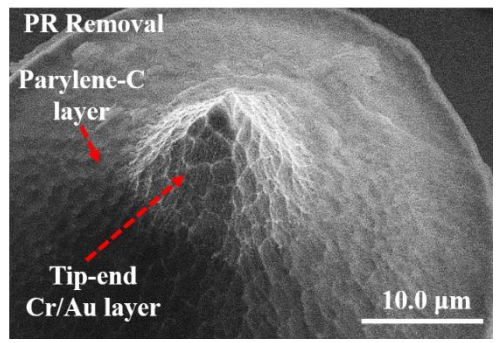

(b) (c)

Figure 3-8. Fabrication results: (a) SEM image of the microprobe tip-end after thick photoresist coating, (b) fabricated MEA, (c) exposed electrode at the tip-end.

The measured microprobe electrode height is 90 µm and the diameter of the conductive layer exposed at the tip end is slightly different for each fabricated microprobe. This is because when the self-alignment process is performed, the photoresist at the tip-end of the microprobe is not completely coated to a uniform thickness on all microprobes. The diameters of the exposed conductive layer of tip-end of microprobe electrodes are summarized in Table 3-2. Figure 3-9 shows the result of wire bonding the MEA array to a printed circuit board (PCB).

Table 3-2. Fabrication results: diameter of the exposed conductive layer.

Exposed conductive layer diameter (μm)	
13.2	14.1
13.4	13.7
13.1	14.3
15.3	22.3
16.1	20.3
20.1	19.5
13.7	18.2
14.2	16.3

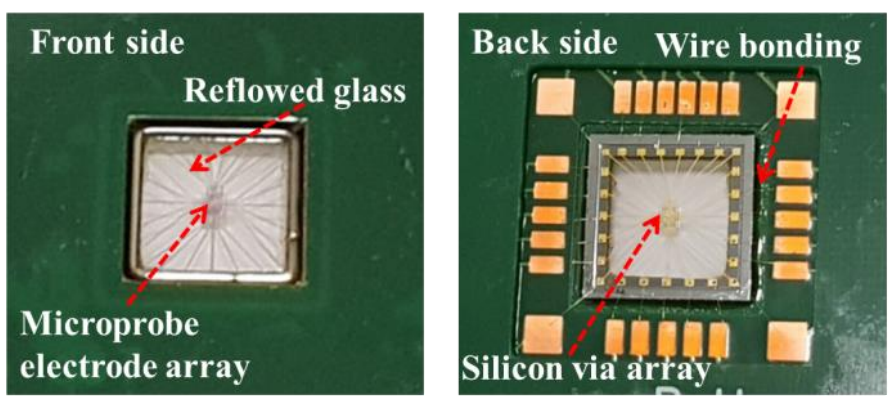

Figure 3-9. MEA connected to a PCB.

The fabricated MEA structure transfers the measurement signal to the backside using a silicon via electrode structure. Thus, the PCB is designed so that the wire bonding process is performed at the backside of the fabricated MEA. First,

the microprobe electrode and the front of the PCB are bonded together using thermal epoxy (353ND, Epoxy Technology) and are cured at 80 ℃ for 1 h. After that, the front side of the PCB and MEA are bonded using epoxy, as in the above method, and then a wire bonding process is performed to electrically connect the microprobe electrode and the PCB. Finally, the backside of the PCB is bonded to prevent damage to the wire bonding area.

3.5. Experiments of light transmittance of fabricated MEA

To verify the transparency of the fabricated microprobe electrode, a light transmittance experiment is performed using a UV/Vis spectrophotometer, (LAMBDA 650, PerkinElmer). Light transmittance tests were performed using a sample subjected to a reflow process at 850 ℃ and 1050 ℃ for 3 h, respectively. The sample used in the experiment is shown in Figure 3-10. To obtain a structure with high transparency by minimizing the crystallization phenomenon occurring during the reflow process, plasma treatment with Cl_2 gas was performed [74].

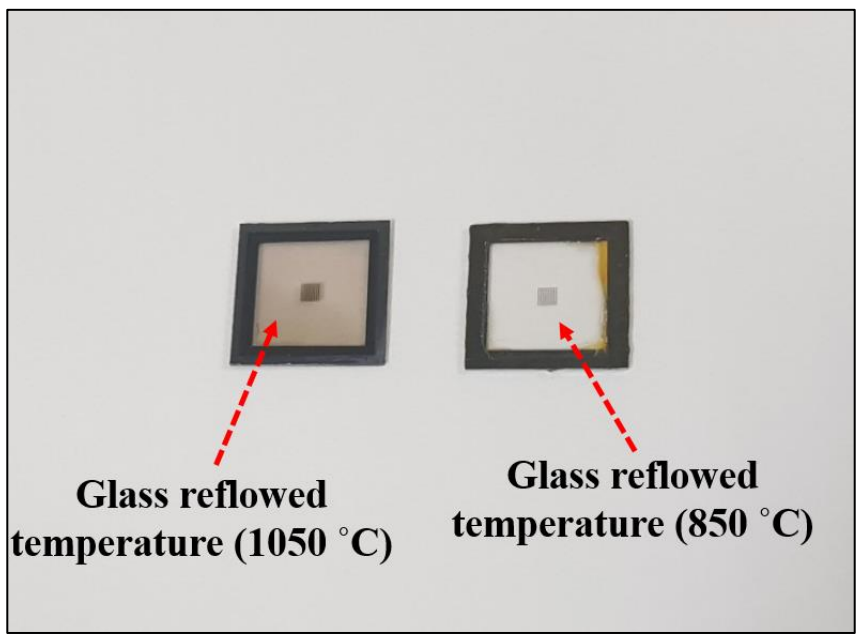

Figure 3-10. Images of experimental samples according to the temperature of the glass reflow process.

The light transmittance measurement results were of 65%–70% at 850 ℃ and 45%–60% at 1050 ℃, as shown in Figure 3-11. These results confirm that the fabricated MEA has high transparency.

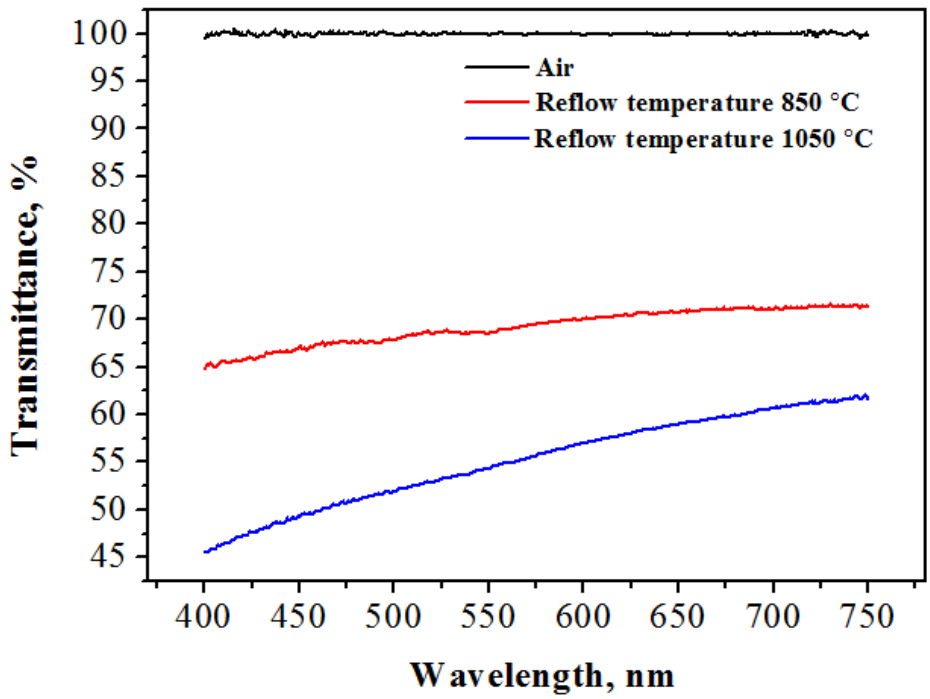

Figure 3-11. Experimental results of light transmittance of fabricated MEA.

With this transparency characteristic, the proposed MEA can be placed at a desired position as the target tissue to be measured is seen through the substrate during the biological experiment, thereby minimizing damage to the tissue.

Chapter 4. Electrochemical measurement

4.1. Introduction

Electrochemical impedance spectroscopy (EIS) and cyclic voltammetry (CV) measurements were performed to verify the electrochemical properties of the MEA.

The CV measurement experiment was carried out to confirm that redox reactions occur at the microprobe electrode and to perform analyses related to the individual measurements. The steady-state limiting current of the microprobe electrode is measured using a CV experiment and compared to the theoretically calculated current. In addition, it has been confirmed that the steady-state limiting current increases proportionally as the number of microprobe electrodes increases, which means that the fabricated microprobe electrode can be used as an electrical individual electrode.

The EIS measurement was performed to measure the impedance value of the microprobe electrode, and the component value of the equivalent circuit of the microprobe electrode was predicted using a z-view simulation. Especially, it has been confirmed that the impedance value at 1 kHz does not exceed 1 MΩ, which makes it suitable for biological experiments [3, 75].

Finally, measurement of a chemical crosstalk that affected the measurement signal during the biological experiment was performed.

4.2. Measurement methods

4.2.1. Impedance measurement method

EIS experiments were carried out to analyze the electrochemical characteristics of the microprobe electrodes fabricated in this study. Based on EIS, a Nyquist plot measurement and an impedance measurement are performed according to frequency variations. First, the Nyquist plot means that the real and imaginary parts are shown in two dimensions on the *x* and *y* axes, respectively, when expressing the measured impedance as a complex function. The Nyquist plot is generally analyzed using an electrochemical equivalent circuit, as shown in the Figure 4-1.

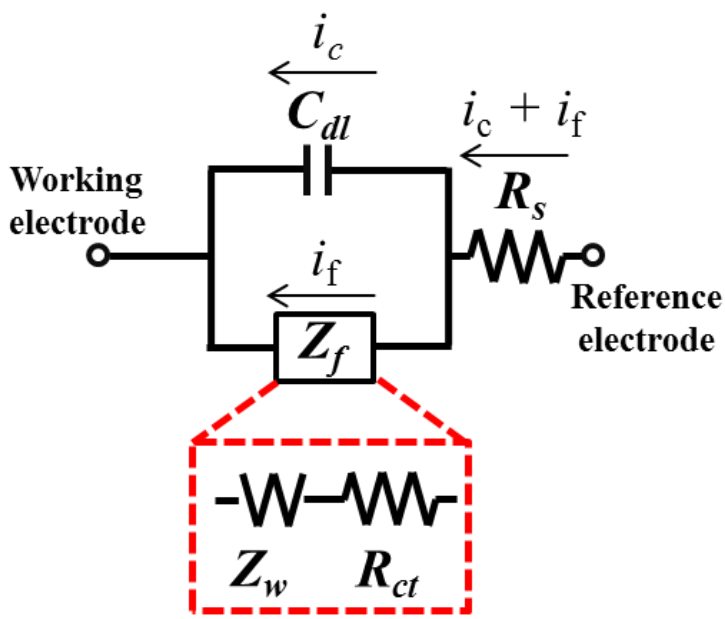

Figure 4-1. Equivalent circuit that describes the current flow between the reference electrode and the working electrode.

In the equivalent circuit, R_s denotes the electrolyte resistance between the working electrode and the reference electrode, and Z_f denotes the impedance of the Faraday reaction. Z_f can be subdivided into circuits in which Z_w and R_{ct} are connected in series.

The total current of the equivalent circuit is the sum of the electric double layer charge current (i_c) and the Faraday current (i_f). Rct is the charge transfer resistance, which means the generated resistance when the charge moves to the electrode. Z_W is given as a function of σ related to mass transfer, which is called Warburg impedance. Z_w can be subdivided into circuits in which R_w and C_w are connected in series. R_w and C_w are expressed as Equation 4-1, where σ and ω are functions related to mass transfer and angular frequency, respectively.

$$R_w = \frac{1}{\omega C_s}, C_w = \frac{1}{\sigma \omega^{1/2}} \tag{4-1}$$

The three impedance values finally obtained by subdividing Z_f vary with frequency. In the case of $\omega \rightarrow 0$, $Z_f = Z_W$ because $Z_W >> R_{ct}$, and when $\omega \rightarrow \infty$, $Z_f = R_{ct}$ because $Z_W << R_{ct}$. Therefore, Z_W related to mass transfer can be obtained in the low-frequency region, and R_{ct} can be obtained in the high-frequency region. The total impedance is $Z = Z_s + Z_{par}$, where Z_{par} is given as Equation 4-2, and Z_f and Z_{Cdl} are expressed as Equations 4-3 and 4-4, respectively.

$$\frac{1}{Z_{par}} = \frac{1}{Z_{C_{dl}}} + \frac{1}{Z_f} \tag{4-2}$$

$$Z_f = R_{ct} + R_w - \frac{j}{\omega C_w} \tag{4-3}$$

$$Z_{C_{dl}} = \frac{-j}{\omega C_{dl}} \tag{4-4}$$

The total impedance is $Z = Z_s + Z_{par}$ divided by the real part and the imaginary part and can be expressed as Equations 4-5 and 4-6, respectively.

$$Z_{Re} = R_s + \frac{R_{ct}+\frac{\sigma}{\omega^{1/2}}}{(C_{dl}\sigma\omega^{1/2}+1)^2+\omega^2 C_{dl}{}^2(R_{ct}+\frac{\sigma}{\omega^{1/2}})^2} \quad (4\text{-}5)$$

$$Z_{Im} = \frac{\omega C_{dl}(R_{ct}+\frac{\sigma}{\omega^{1/2}})^2+\frac{\sigma}{\omega^{1/2}}(\omega^{1/2}C_{dl}\sigma+1)^2}{(C_{dl}\sigma\omega^{1/2}+1)^2+\omega^2 C_{dl}{}^2(R_{ct}+\frac{\sigma}{\omega^{1/2}})^2} \quad (4\text{-}6)$$

The change in impedance owing to the frequency change is shown in Figure 4-2. It can be seen that as the frequency changes from high to low, the impedance increases linearly because, when ω goes to zero, the Z_{re} and Z_{Im} equations are converted to Equations 4-7 and 4-8, respectively.

$$Z_{Re} = R_s + R_{ct} + \frac{\sigma}{\omega^{1/2}} \quad (4\text{-}7)$$

$$Z_{Im} = 2\sigma^2 C_{dl} + \frac{\sigma}{\omega^{1/2}} \quad (4\text{-}8)$$

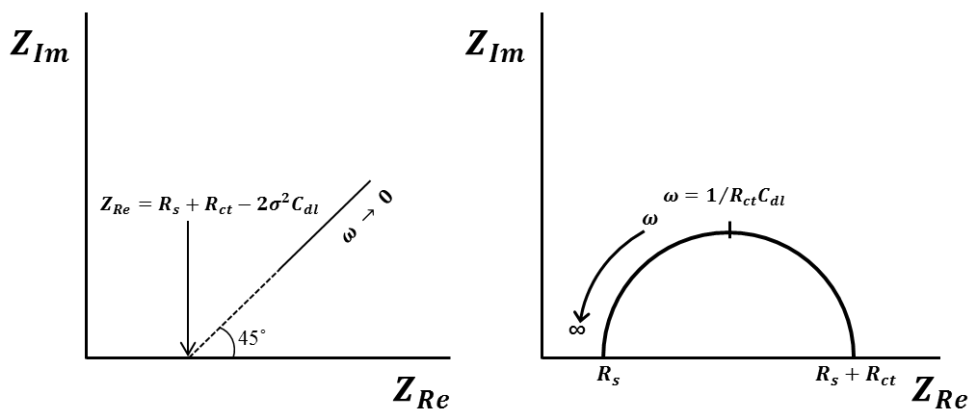

(a) (b)

Figure 4-2. Change in impedance owing to frequency variation: (a) impedance change in the low-frequency region, (b) impedance change in the high-frequency region.

As the frequency increases, the value of the impedance changes in a semicircular shape, because, when ω goes to zero, the Z_{re} and Z_{Im} equations are converted to Equations 4-9 and 4-10, respectively.

$$Z_{Re} = R_s + \frac{R_{ct}}{1 + \omega^2 {R_{ct}}^2 {C_{dl}}^2} \tag{4-9}$$

$$Z_{Im} = \frac{\omega {R_{ct}}^2 C_{dl}}{1 + \omega^2 {R_{ct}}^2 {C_{dl}}^2} \tag{4-10}$$

Impedance graphs can be represented in all frequency ranges by combining the impedance graphs at the low and high frequencies of Figure 4-2, as shown in Figure 4-3.

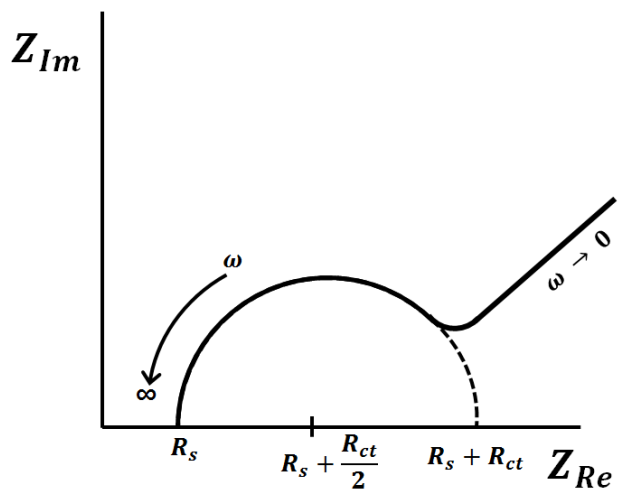

Figure 4-3. Impedance change in the low-frequency and high-frequency regions.

Using this graph, various types of values of the equivalent circuit can be obtained from the x-intercept of the Z_{re} axis, and the electrochemical characteristics can be analyzed.

4.3. Measurement results

4.3.1. Individual electrode measurement using CV experiment

CV measurement was performed to examine the electrochemical properties of the fabricated MEA. Figure 4-4 shows the experimental setup configuration for CV measurements. The CV measurement is performed by the three-electrode measurement method using a potentiostat (VersaSTAT 3, Princeton Applied Research). The microprobe electrode is bonded to the PCB board, the PDMS-based well is bonded on the microprobe electrode, and then the experiment is conducted using the acrylic jig. The whole area of the MEA is positioned inside the PDMS-based well filled with ferricyanide and KCl solution. The MEA is used as the working electrode, Pt wire as the counter electrode, and Ag/AgCl as the reference electrode, respectively. The CV measurement was recorded at 50 mV/s scan rate with a voltage range from −0.7 V to 0.7 V.

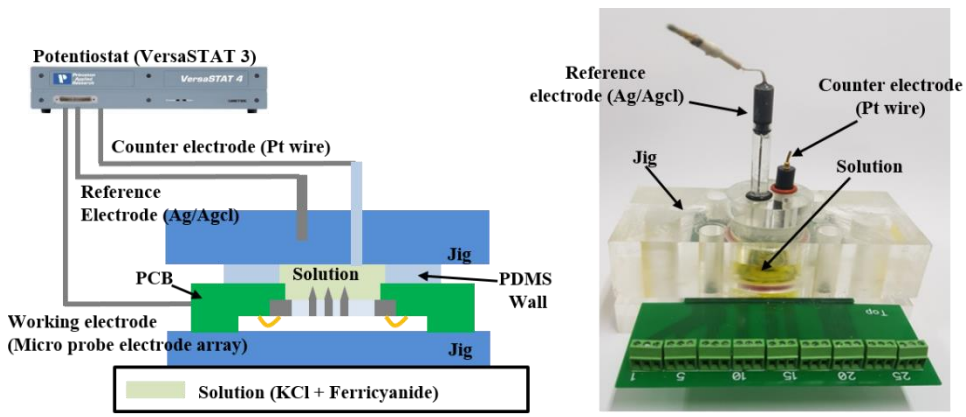

(a) (b)

Figure 4-4. (a) CV measurement setup of MEA combined with PCB, (b) assembled package in the acrylic jig including the electrodes and the PDMS well filled with solution.

To investigate the microelectrode characteristics of the MEA, a CV measurement was performed using one probe electrode. Experiments were carried out using 0.1 M, 0.4 M ferricyanide and 0.1 M KCl solutions on one probe electrode. The measurement results are shown in Figure 4-5. The CV results exhibit the typical behavior of UMEs, and it can be seen that the measured current increases proportionally with the concentration of ferricyanide solution.

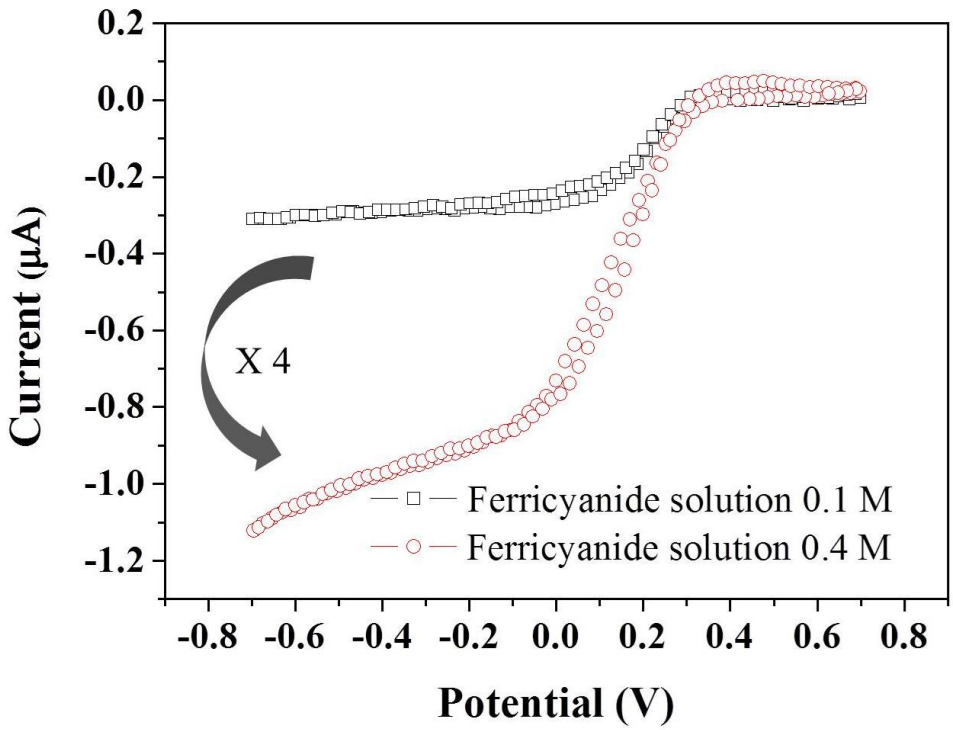

Figure 4-5. CV measurement results using the fabricated MEA with different ferricyanide concentration.

To analyze the CV measurement results, the experimental results were compared with the theoretically calculation results of the steady-state limiting current in the conductive layer exposed at the tip-end of the microprobe electrode. For the theoretical calculation of the steady-state current, the analysis was

performed using the theory applicable to most conical micro electrode structures studied by Leonhardt et al. [76]. Leonhardt reports that the steady-state limiting current varies with insulation angle and thickness. The steady-state limiting current changes because if the insulation thickness has small values, the amount of back diffusion around the insulation coating can be controlled according to the insulation angle, so that the value of the steady-state limiting current can be changed. As the microprobe structure fabricated in this study also uses a thin film of 3000 Å of Parylene-C as the insulation layer, it can be analyzed with Leonhardt's results. The following equations are applicable to obtain the steady-state limiting current:

$$i_{tip} = nFDc^{b}r_{tip}[A_H + B_H(R_g + C_H)^{-D_H}] \quad (4\text{-}11)$$

In Equation (4-11), n is the number of electrons transferred during the reaction, *F* is the Faraday constant, and *D* is the diffusion coefficient of the ferricyanide solution. c^b is the bulk concentration, and r_{tip} is the diameter of the cone of the fabricated microprobe. R_g is the radius of the insulation sheath, which is the ratio of the insulation layer thickness to the radius of the microprobe. Equations (4-12) to (4-15) are parameters calculated by simulation, and the values are changed based on the *H* value, which is the aspect ratio of the conical tip structure.

$$A_H = 1.47972H + 3.69141 \quad (4\text{-}12)$$

$$B_H = 0.12629H^2 + 0.65894H - 0.01259 \quad (4\text{-}13)$$

$$C_H = 0.0115H^2 + 0.25251H - 0.72687 \quad (4\text{-}14)$$

$$D_H = -0.00943H^2 + 0.08213H + 0.83038 \quad (4\text{-}15)$$

Table 4-1 summarizes the parameters for calculating the above formulae. The steady-state limiting current values of the microprobe electrode array calculated using the above equations and parameters were compared with the values measured

at 0.1 M and 0.4 M. As a result, the difference between the theoretical and measured values is not large, and it can be seen that the fabricated microprobe electrode well as the microelectrode, as presented in Table 4-2.

Table 4-1. Parameters used in the calculation of the steady-state limiting current.

Parameters	**Value**	**Units**
Faraday constant (F)	9.65×10^{4}	$Cmol^{-1}$
Diffusion coefficient (D)	7.00×10^{-6}	$cm^{2}s^{-1}$
Bulk concentration (c^{b})	100	mM
Aspect ratio (H)	1.06	
Radius of the insulation sheath (R_g)	1.04	

Table 4-2. Comparisons of measured currents with estimated values

Concentration of ferricyanide solution, M	**Current**		
	Estimated value, nA	**Measured value, nA**	**Error, %**
0.1	298.1	244.8	17
0.4	1192.4	1113	6

Additional CV experiments were performed to verify that the microprobe electrodes could be used as individual electrodes. The fabricated microprobe electrode has a structure in which the reflowed glass is filled between the silicon via electrodes, and the microprobe electrode is located on the silicon via and can be completely separated electrically and used as an individual electrode. In total, 8 of the 16 electrodes were used to verify the properties of these structures through electrochemical experiments. The concentration of the ferricyanide solution is fixed at 0.1 M under the same condition as that in the above experiment.

The experimental method is as follows. First, the CV of one microprobe electrode is measured, and then the number of microprobes is increased by one. At this time, it is verified whether the current value increases in proportion to the number of electrodes in the CV measurement. It can be seen that the fabricated microprobe electrode works well as an individual electrode by confirming the magnitude of the current produced by the added electrode. Figure 4-6 shows the CV measurement results from increasing the number of microprobe electrodes individually connected to the potentiostat.

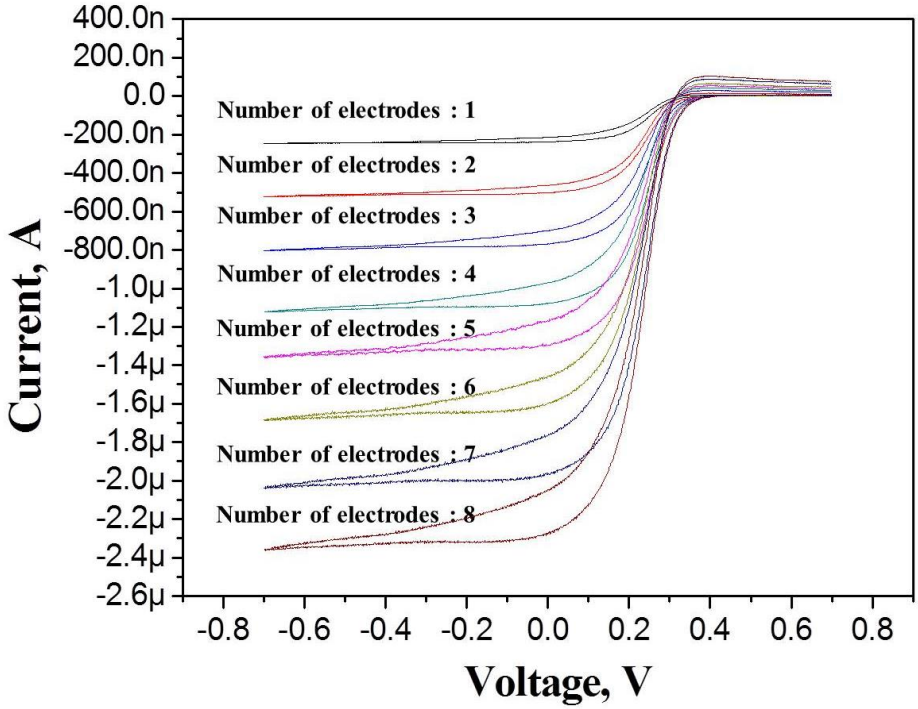

Figure 4-6. CV measurement results by increasing the number of individual microprobe electrodes connected to the potentiostat through the silicon TGVs.

The graph of the measured current has confirmed that it has a typical microelectrode current characteristic. The measured peak current values according to the number of microprobe electrodes are listed in Table 4-3. In the measurement results, the peak current value of the steady-state limiting current is slightly different for each electrode. This is because the exposed height of the conductive layer of the microprobe electrode is slightly different in the Parylene-C etching process. From these results, it can be seen that the conductive layer was successfully exposed only at the tip-end and the MEA was successfully fabricated as an individual electrode.

Table 4-3. Measured peak currents by increasing the number of individual microprobe electrodes connected to the potentiostat.

Number of electrodes	**Measured Current (nA)**
1	244.8
2	521.6
3	807.7
4	1100.7
5	1398.3
6	1730.7
7	2070.4
8	2401.3

4.3.2. Impedance measurement result

EIS measurements were performed by varying the frequency and simultaneously measuring the impedance resistance, phase, and Nyquist plot of the electrode. A single microprobe EIS measurement uses a 3 M KCl solution with a measurement frequency range from 0 to 10 kHz. The measurement results are shown in Figure 4-7. To analyze the measurement results, the analysis was carried out by using the Randles equivalent circuit model, which can model the microprobe in the electrolyte solution.

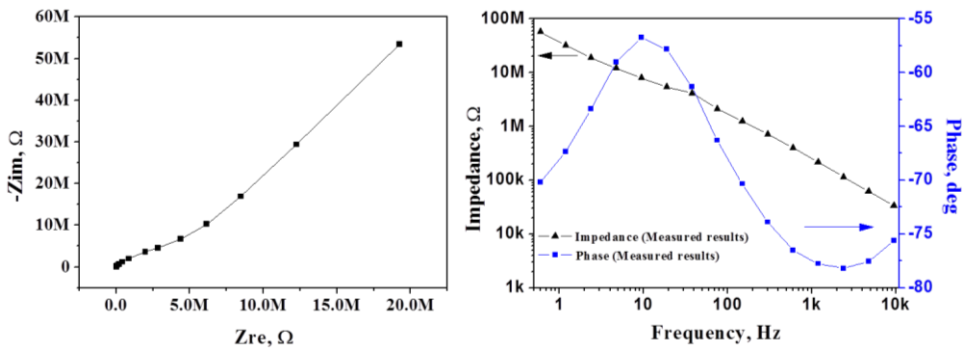

(a) (b)

Figure 4-7. Impedance measurements of microprobe electrode: (a) Nyquist plot, (b) measured impedance and phase of the microprobe electrode at various frequencies.

The value of the equivalent circuit component can be obtained by fitting the measured impedance data using the Zview modeling program. The fitting results using the Zview software are shown in Figure 4-8. The estimated equivalent circuit component values are summarized in Table 4-4. R_{ct} is the resistance generated when the charge moves to the electrode, and R_s is the resistance between the working electrode and the reference electrode in an aqueous solution. The constant

phase element (CPE) is related to the double-layer capacitor and consists of CPE-T and CPE-P. The CPE concept is expressed in the following Equation 4-16:

$$Z(CPE) = 1/[T(\mathrm{j}\omega)^{P}] \quad (4\text{-}16)$$

Where j is the imaginary number, ω is the angular frequency, and T is the CPE-T, which is the capacitance value of the CPE-T. *P* has a value between 0 and 1, which means that CPE-P and is a factor caused by surface roughness, reaction rate, and thickness change. If *P* is 1, the CPE can be defined as the perfect electrical double layer (EDL) [77, 78]. The value of CPE-P calculated using the Zview simulation of the fabricated microprobe electrode is 0.88. As a result, the CPE value can achieve a nearly perfect double-layer capacitor value. W is the Warburg impedance, which is a factor resulting from the mass transfer of the electrode.

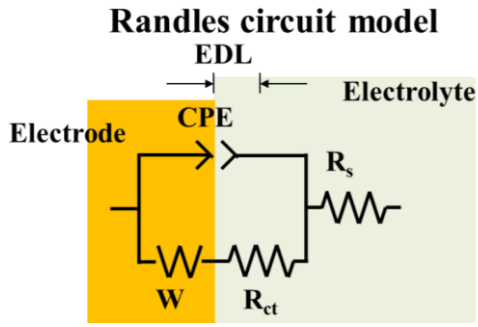

(a)

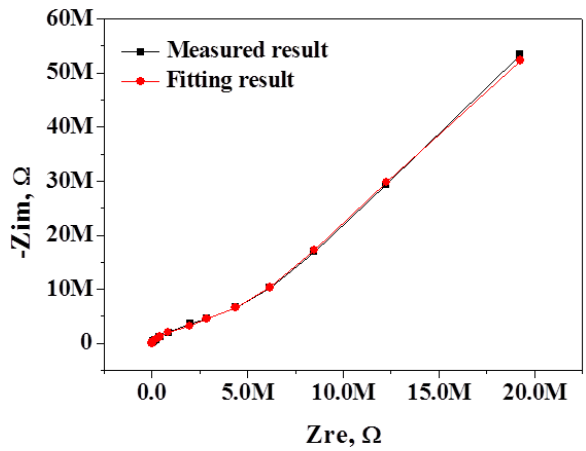

(b)

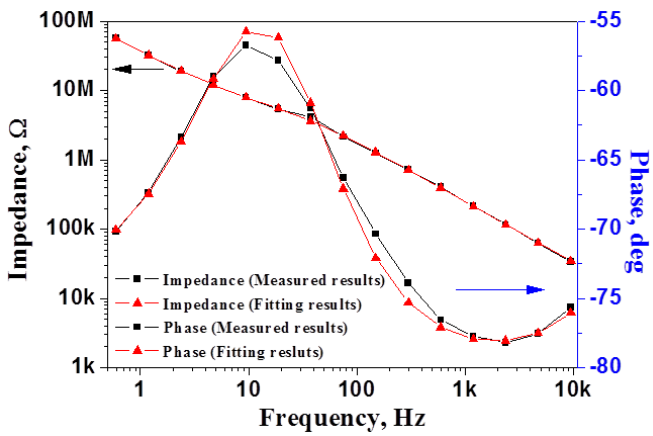

(c)

Figure 4-8. Measured impedance analysis: (a) Randle circuit model, (b) fitting results of Nyquist plot using Zview modeling program, (c) fitting results of impedance and phase change.

Table 4-4. Individual component values of an equivalent circuit.

Components	**Value**	**Units**
Solution resistance (R_s)	2.18	kΩ
Charge transfer resistance (R_{ct})	8960	kΩ
Warburg impedance (Z_w)	49.2	MΩ
Constant phase element (CPE-T)	1.72	nF
Constant phase element (CPE-P)	0.88	

The previous studies have reported that in *in-vitro* experiments, the impedance value should be less than 1 MΩ at 1 kHz to measure individual neural signals with high SNR [3, 75]. Based on previous studies, the impedance of the fabricated microprobe electrode was measured at 292 ± 156 kΩ at 1 kHz, which was sufficiently low to detect individual neural signals with a high SNR.

4.3.3. Electrochemical crosstalk

Many studies have been conducted by numerous researchers to reduce the loss of signals measured in bio-experiments. One of the primary factors in determining the quality of a measured signal is chemical crosstalk. To improve the quality of the measurement signal on individual electrodes it is important to minimize the chemical crosstalk that affects it. Chemical crosstalk is mainly affected by the distance between the electrodes. It has been reported that the distance between adjacent electrodes should be at least 100 μm to minimize chemical crosstalk [5, 79].

In the proposed microprobe structure, the distance between adjacent electrodes is 210 μm, and experiments are carried out to measure the chemical crosstalk between the electrodes. Two adjacent probe electrodes are used. One of the electrodes is set as a generating electrode that generates electro-active species, and the other electrode is set as a monitoring electrode for measuring chemical crosstalk. The solution used in the experiments to measure chemical crosstalk is ferricyanide ($Fe(CN)_6^{3-}$), as shown in Figure 4-9(a).

First, the voltage between the monitoring electrode and the Ag/AgCl electrode as the reference electrode is fixed at a voltage of 0.3 V and the current is measured. Then, voltages of −0.2 V, −0.4 V, −0.6 V, and −0.8 V are applied to the generating electrode and the current value generated from the monitoring electrode is measured. In the process, Ferrocyanide ($Fe(CN)_6^{4-}$) is produced by the reduction reaction occurring at the generating electrode.

The generated $Fe(CN)_6^{4-}$ diffuses into the monitoring electrode and the oxidation reaction generates $Fe(CN)_6^{3-}$. At this time, chemical crosstalk current

occurs at monitoring electrode. The measurement result is shown in Figure 4-9(b). First, for a stable measurement of chemical crosstalk, the measurement is performed during 100 s, saturating the measured current at the monitoring electrode, and the above-mentioned voltage is applied to the generating electrode for 20 s each time.

As a result, it was confirmed that even if a voltage was applied to the generating electrode, the current value at the adjacent monitoring electrode did not change. Therefore, there is no chemical crosstalk in the fabricated electrode.

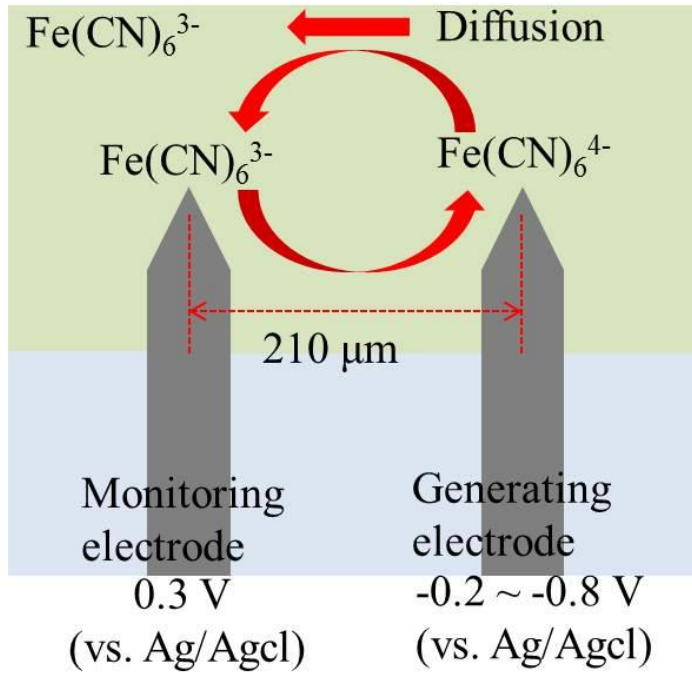

(a)

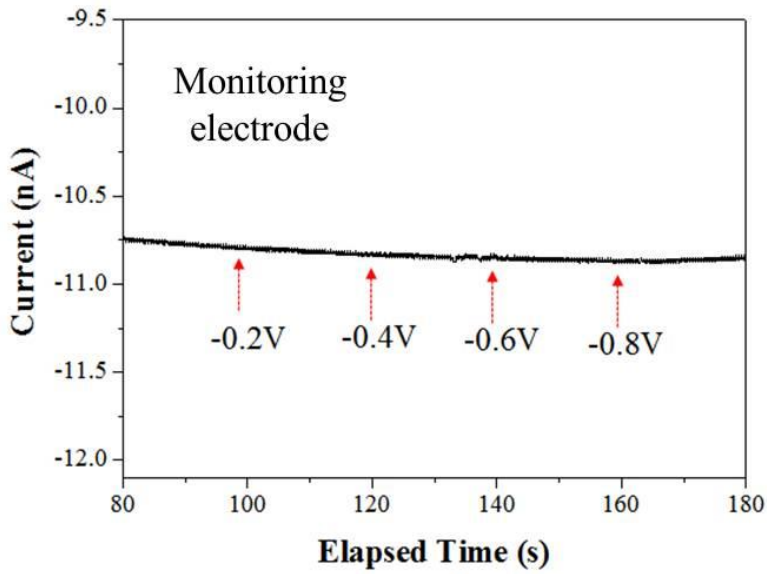

(b)

Figure 4-9. Chemical crosstalk experiment: (a) measurement setup, (b) experiment result.

Chapter 5. *In-vitro* experiment

5.1. Introduction

In-vitro experiments were performed to verify that neural spike signals can be successfully measured using the fabricated microprobe electrode. Based on our previous study, we included a more detailed experimental method and conducted an experiment and analysis using a hippocampal brain slice [69].

After primary rat neuron cells are cultured on the fabricated microprobe electrode, neural spike signal measurement was performed to verify the individual and high SNR signal measurements.

The measurement and analysis of the neural spike signals using a rat hippocampal brain slice tissue are described in Section 5.3. The microprobe electrode was inserted into the tissue through the dead cell layer of the hippocampal brain slice to verify that the neural spike signal could be measured.

5.2. Measurement of neural spike through culturing of rat cortical neuron cells

5.2.1. Device design and fabrication

The device design for the measurement of neural signals was based on the fabricated MEA. To measure the neural spike signal at each electrode, the fabricated microprobe electrodes were patterned into a 4 x 4 array. The PCB was designed to transfer the measured signal to the external measuring equipment.

The PCB and the fabricated MEA are attached using thermal epoxy (353ND, Epoxy Technology) and treated at 80 ℃ for 1 h to fix them firmly. The system was then configured to connect to the RHD2000 USB interface board, a measurement signal processing module, using a 16-channel connector (A79038-001, Omnetics Connector Corporation), as shown in Figure 5-1(a). There is a microprobe electrode in the center of the device, and a Pt wire is connected to both ends of the device. These electrodes are used as the working and reference electrodes, respectively. A 15 mm × 15 mm PDMS chamber is attached to the MEA fabricated for neuron culture, as shown in Figure 5-1(b).

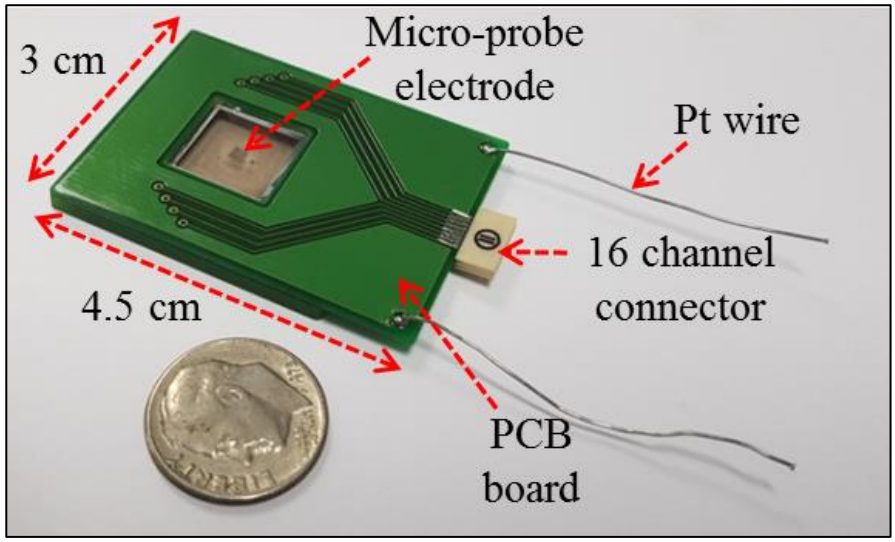

(a)

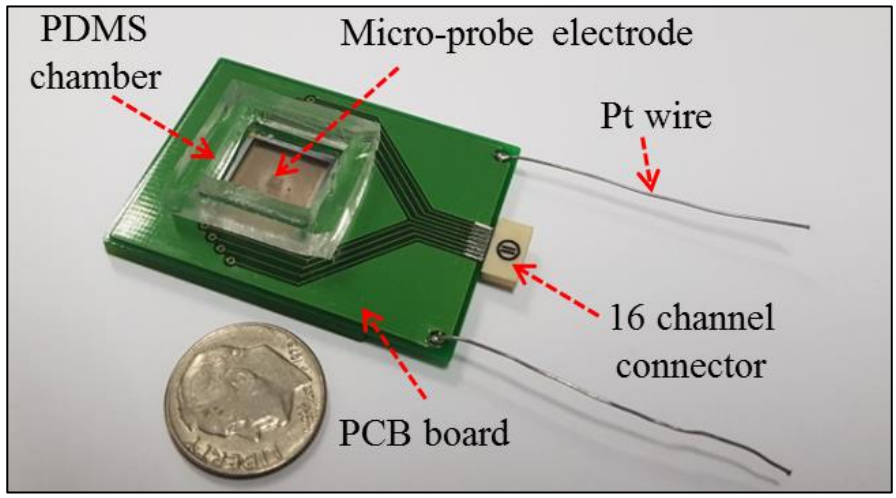

(b)

Figure 5-1. MEA device for measurement of cultured neuron signal: (a) MEA combined with PCB board, (b) MEA device with a PDMS chamber for neuronal cell culture.

5.2.2. Cell culture method

For seeding neurons, the microprobe electrode and the PDMS chamber are cleaned with 70% ethanol for 30 min and rinsed three times for 20 min using deionized water. Then, the microprobe electrode was treated with O2 plasma (80 W, 40 s), and poly-D-Lysine treatment for cell adhesion was performed for 3 h in a CO_2 incubator (Sanyo, Japan). The MEA was treated with UV light overnight in the hood. We used rat embryos for isolation and culture of primary neurons. Pregnant Sparague Dawley rats (E17) were purchased from DBL (Eumseong, South Korea) and all culture processes were conducted in accordance with the ethical standards stated in the animal welfare guidelines of the Korea Institute of Science and Technology (KIST, South Korea). Primary neural cultures were performed using previously reported cell culture protocols [80]. Briefly, the brain was extracted from the rat embryo and the entire cortex was dissected out. The whole cortex was treated with papain for isolation, and the cells were seeded on the PDL-coated microprobe at a density of 2500/mm^2 with 1 ml of culture media. The culture media consisted of neurobasal media supplemented with 2% of B27-supplement (Invitrogen, United States), 2 mM of Glutamax-I (GIBCO, United States), and 1% of penicillin–streptomycin (GIBCO, United States). One-half of the medium was replaced with fresh medium every 3 days.

5.2.3. Measurement method

Seven days after the culture, the experiment was carried out with a MEA in which neuron cells were cultured. Figure 5-2(a) shows the schematic view of the measurement setup. First, the Pt-wire connected to the PCB was immersed in the culture medium. Extracellular recording amplified the signal through the RHD2132 amplifier board and the signal was transferred through the SPI cable to the RHD 2000 USB interface board to analyze it with a PC. The amplifier board was connected to the MEA via a 16-channel connector, as shown in Figure 5-2(b). The recorded neural signals were amplified (192 V/V), band-pass filtered (300–6000 Hz), and digitized at 20 kS/s per channel with 16-bit ADC. Spontaneous neuronal activity was recorded for 10 min from the rat primary cortical neurons seven days after seeding the cells on the microprobe electrode. To analyze the recorded data, spike sorting was performed by a customized sorting algorithm (The Mathworks) [3]. The customized algorithm is based on amplitude thresholding, which is a widely used method to classify the spikes by amplitude [81]. The threshold amplitude was set based on the previously reported methods [82, 83]. Briefly, the SNR was calculated by dividing the peak amplitude of the detected signals by three times the standard deviation of the noise amplitude. Then, the spike with an SNR of 1.25 or more was classified as a neural spike.

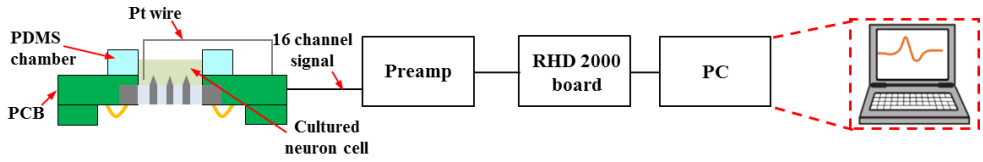

(a)

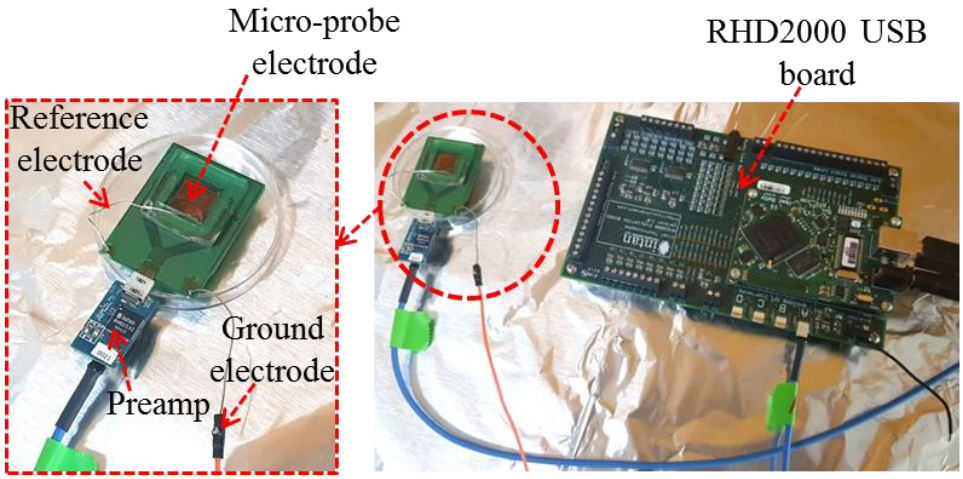

(b)

Figure 5-2. Measurement method: (a) schematic view of the measurement setup, (b) preamplifier (RHD 2132) and microprobe electrode connected via a 16-channel connector.

5.2.4. Measurement results and analysis

Neural signals were successfully recorded using the fabricated microprobe electrodes. Figure 5-3 shows the result of measuring the signal for 10 min at 16 electrodes. As a result, neural spike signals were measured at all 16 electrodes. As shown in Figure 5-3(a), among the 16 electrodes, many neural spike signals were measured at the E9 electrode, and the detailed analysis was performed using this electrode. Spike detection was performed using a customized algorithm (Matlab, Mathworks) to determine the number of nerve spike signals generated at each electrode. Figure 5-3(b) presents the result of a raster plot of this spike detection. In the E9 electrode, the measurement signal can be divided into the random spike and burst activity regions according to the number of spike occurrences, as shown in Figure 5-4(a) These areas are evidence that the cultured neurons are healthy and interconnected. For a more detailed analysis, a customized sorting algorithm was used for spike sorting and for size and shape analysis of the neural spike signals measured at the burst activity region of electrode E9. The results of the analysis show that three different action potentials were measured at electrode E9, as shown in Figure 5-4(b), which indicates that three different neurons can be successfully measured at one electrode. The average SNR of the neural spikes measured on the 16 microprobe electrodes was 14.4. This SNR was found to be relatively higher than that of the neural probe electrodes of other research groups [14, 15, 48, 84-88], as shown in Figure 5-5. It can be seen that similar neural spike signals were measured at the other electrodes. These synchronized activities may result from cluster formation and the development of a local neural network among neurons as the cell grows during the incubation period of seven days [89]. Based on these

results, it was confirmed that the microprobe electrode can be used as a biomedical application capable of recording neural signals.

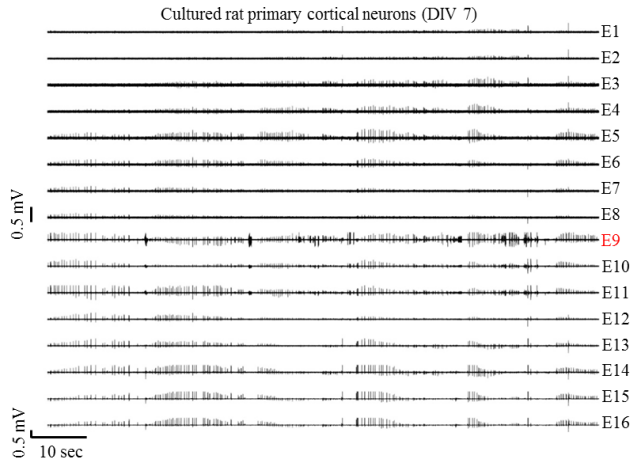

(a)

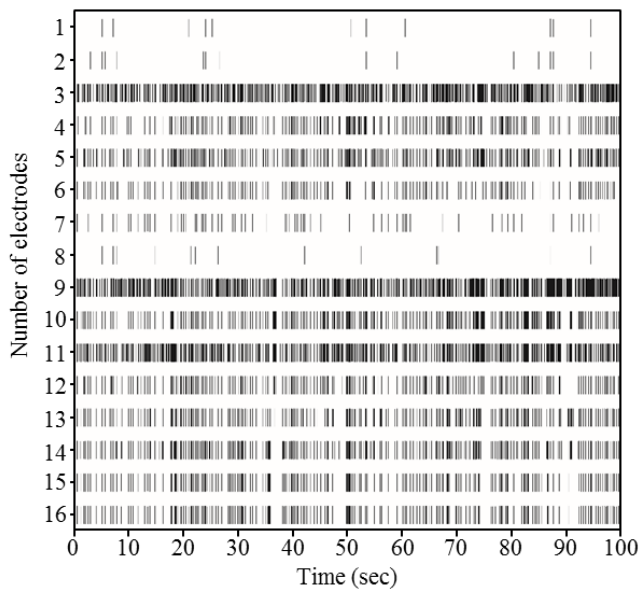

(b)

Figure 5-3. *In-vitro* experimental results using MEA: (a) transient plot of neural signals from cultured rat primary cortical neurons (DIV 7) measured using the microprobe electrode, (b) Raster plot of extracted neural signals from 16 electrodes.

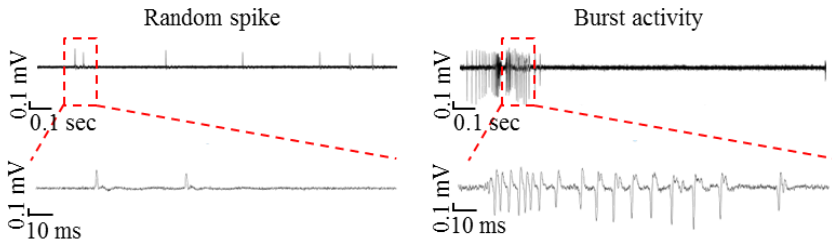

(a)

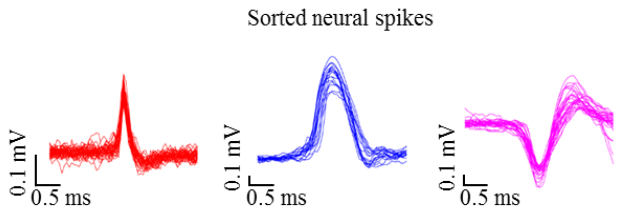

(b)

Figure 5-4. Neural spike signal analysis: (a) close-up transient plots of neural signals measured from E9, (b) sorted neural spikes of three different neurons from E9.

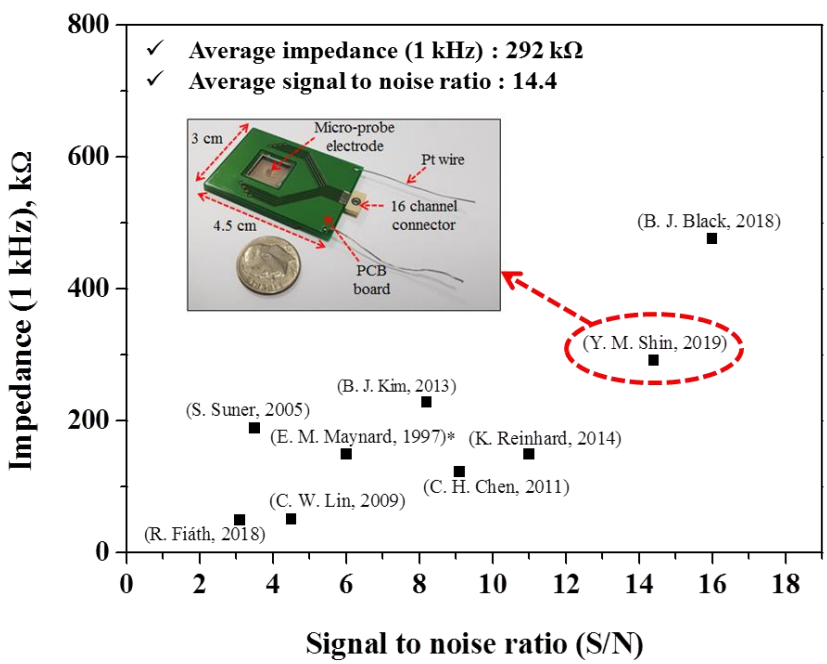

Figure 5-5. Impedance and SNR comparison with conventional research.

5.3. Measurement of neural signal in rat hippocampal brain slice tissue

5.3.1. Device design and fabrication

To perform experiments using a mouse hippocampal brain slice tissue, the probe height of the microprobe electrode was fabricated to have an average height of 190 μm, as shown in Figure 5-6. This is because the probe must be high enough to penetrate the dead cell layer of the hippocampal brain slice tissue and be inserted into the tissue.

Then, the experiment is performed using a MEA recording system (USB-ME64-System, Multi-channel system), and the PCB is also designed to match the form factor of the equipment. The fabricated device is shown in Figure 5-7. The PCB and microprobe electrodes are attached using thermal epoxy. Then, an Au wire bonding process is performed to connect the microprobe electrode to the PCB. The size of the fabricated device was 5 cm × 5 cm and a Teflon ring chamber with a height of 6 mm was attached to the center of the device. The number of measurement electrodes is 16 and one Pt-wire is used as a reference electrode.

Impedance measurements were performed to verify the electrochemical properties of the fabricated microprobe electrode. The measurement was carried out using a 3 M KCl solution. Pt-wire was used as the counter and reference electrode, and the microprobe electrode was used as the working electrode. As a result, it was confirmed that the average value of the impedance at 1 kHz measured at the 16 electrodes was of 0.289 ± 0.145 MΩ.

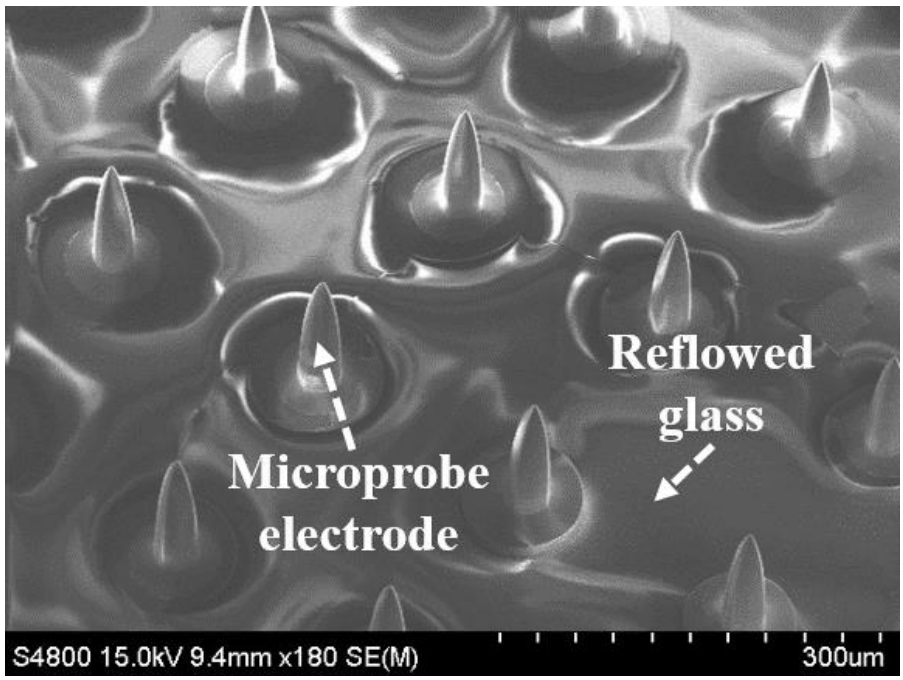

Figure 5-6. SEM image of MEA with probe height above 190 μm.

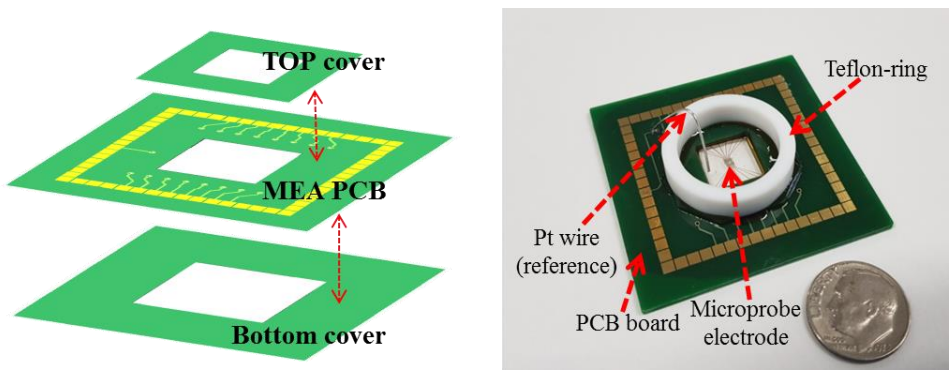

Figure 5-7. MEA device for measurement of hippocampal brain slice tissue.

5.3.2. Measurement method

We used a young mouse for hippocampal brain slice recording. A C57BL/6 mouse (male, 3 weeks) was purchased from Samtako Inc. (Osan, South Korea) and all processes were conducted in accordance with the ethical standards stated in the animal welfare guidelines of Ewha Womans University (Seoul, South Korea). The hippocampal brain slice was performed according to the previously reported organotypic slice protocol [90].

The animal was anesthetized with isoflurane before decapitation, and the brain was rapidly removed and sliced in an ice-cold solution containing 86 mM NaCl, 3.0 mM KCl, 1.0 mM NaH_2PO_4, 20 mM $NaHCO_3$, 1.0 mM $CaCl_2$, 4.0 mM $MgCl_2$, 25 mM glucose, and 75 mM sucrose (saturated with 95% O_2 and 5% CO_2, pH = 7.3). Slices were cut at 300 μm coronal sections using a vibratome (Vibratome). The slices were stabilized in artificial cerebrospinal fluid (ACSF) containing 124 mM NaCl, 4.5 mM KCl, 1.2 mM NaH_2PO_4, 26 mM $NaHCO_3$, 2.0 mM CaCl2, 1.0 mM $MgCl_2$, and 10 mM glucose at room temperature (saturated with 95% O2 and 5% CO2, pH = 7.3). Then, an experiment was carried out to insert the microprobe electrode into the hippocampal brain slice tissue. As the microprobe structure is made of a silicon base, it has the disadvantage that it is fragile if physical force is applied. In this experiment, a mouse hippocampal brain slice was carefully placed on a microprobe electrode, which could be inserted into the tissue by pressing it using a 1% agarose gel block. As shown in Figure 5-8, the microprobe electrode was successfully inserted into the hippocampal brain slice tissue without damage.

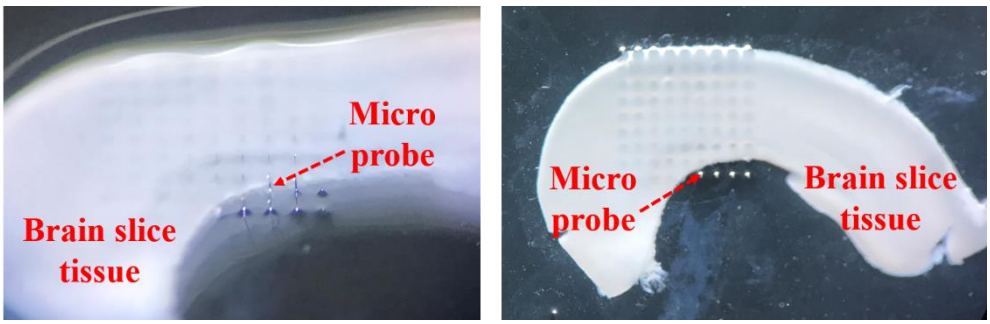

Figure 5-8. Image of microprobe electrode inserted into hippocampal brain slice tissue.

The fabricated microprobe electrode had characteristics of transparency because the substrate was composed of reflowed glass. This transparency property has the advantage that the target tissue can be seen through the glass substrate from the backside of the electrode, as shown in Figure 5-9. In addition, the microprobe electrode can be inserted at a desired position of the target tissue, thereby minimizing damage to the tissue.

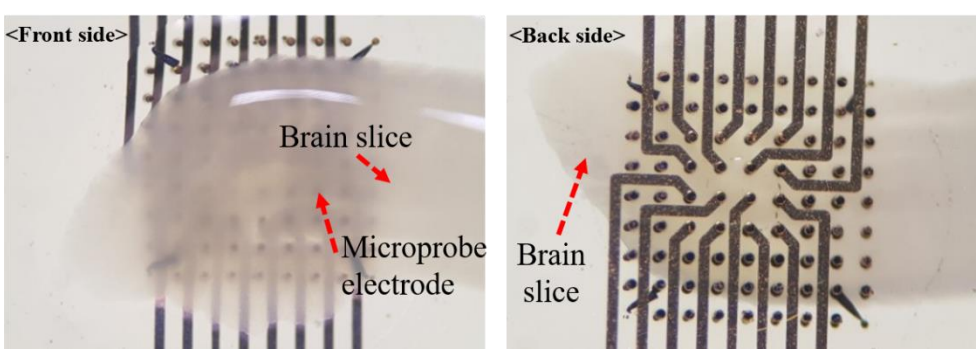

Figure 5-9. Optical microscope image of the front and back sides of the MEA after inserting it into the hippocampal brain slice.

After inserting the microprobe electrode into the hippocampal brain slice tissue, the MEA device is loaded into the multichannel system and the measurement is performed, as shown in Figure 5-10(a). To maintain the solution temperature at 30 ℃ (saturated with 5% CO_2 and 95% air) during the experiment, the solution was circulated inside the Teflon chamber at a flow rate of 0.5 ml/min using the perfusion system (PPS2, Multichannel system), as shown in Figure 5-10(b). The Multichannel system (MC_Rack, Multichannel system) software was used to measure the spontaneous neural activity of the 16 channels.

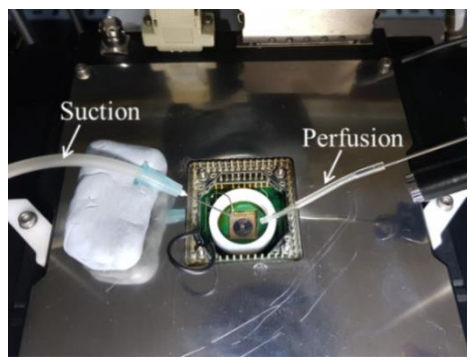

(a)

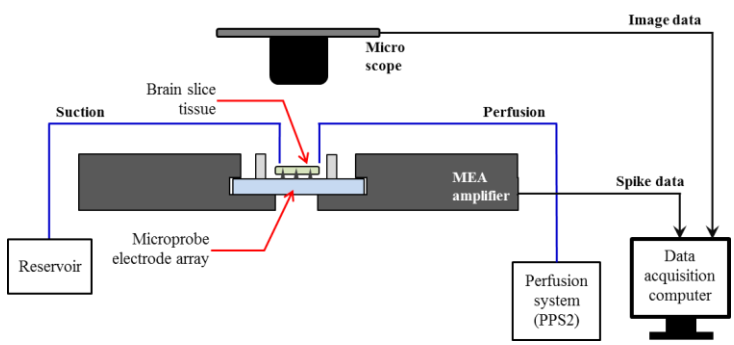

(b)

Figure 5-10. (a) perfusion and suction system, (b) Schematic view of the measurement setup.

5.3.3. Measurement results and analysis

The experimental results are shown in Figure 5-11. It was confirmed that the neural spike signal was successfully measured in 13 out of 16 electrodes. Figure 5-11 shows the location of the microprobe electrode inserted in the hippocampal tissue.

The neural spike train signals measured at each electrode show that signals are generated at similar times. This is because when the neurons inside the hippocampal tissue were fired, the generated signal was measured simultaneously at each electrode.

After measuring the neural spike signals, the electrodes were cleaned with acetone for 5 min and impedance measurements were performed, as shown in Figure 5-12. As a result, the impedance value of 16 electrodes at 1 kHz was measured as 0.288 ± 0.117 MΩ. The impedance measurements showed no significant difference from the impedance values before the *in-vitro* measurement.

These impedance measurement results show that the microprobe electrode was not damaged after the *in-vitro* test and that the three electrodes without measured neural signals were not properly inserted into the hippocampal brain slice.

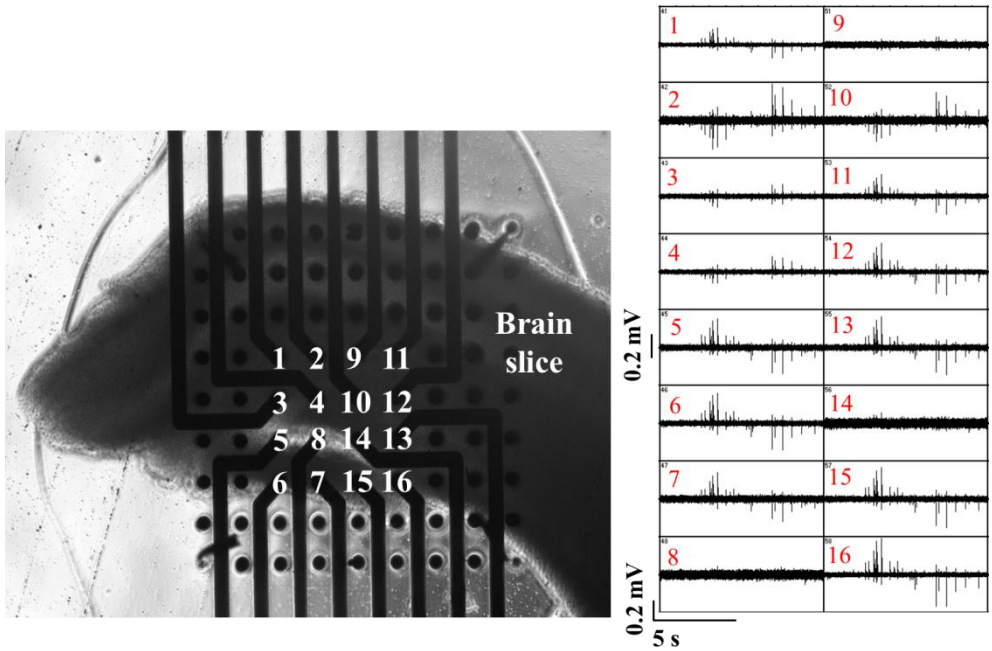

Figure 5-11. The neural spike train measurement result of hippocampal brain slice tissue.

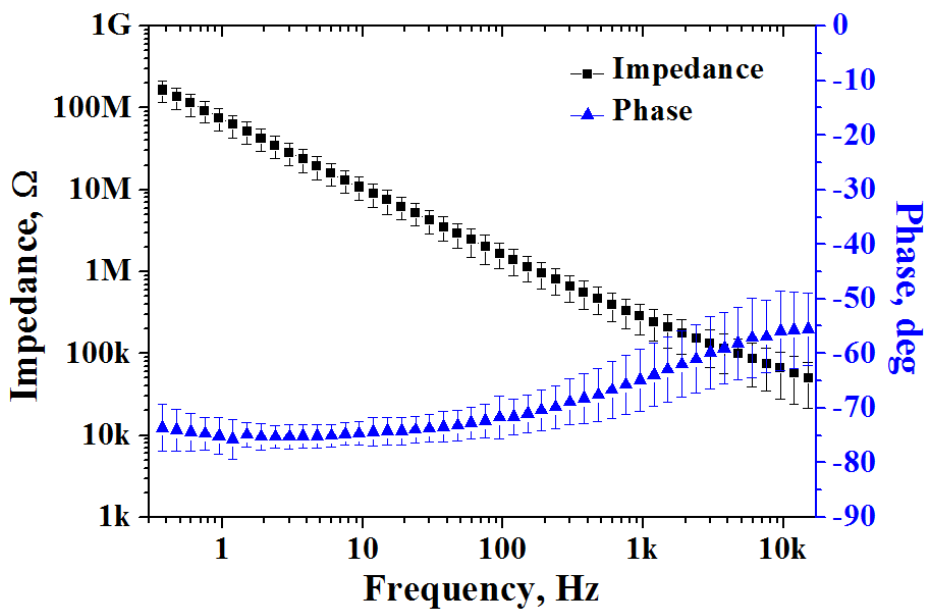

Figure 5-12. Impedance measurement results of microprobe after insertion in hippocampal brain slice.

To analyze the measured signals, a spike sorting process was performed using the MC_Rack software (Multichannel system, USA). As a result of the spike sorting, it can be confirmed that the action potentials measured at the 13 electrodes had similar shapes and that the action potential of two different neurons was successfully measured at each electrode, as shown in Figure 5-13. This result indicated that the neural signal fired from the neuron was successfully measured simultaneously on multiple electrodes. It was confirmed that the SNR of the measured neural signal has a maximum value of 10 or more.

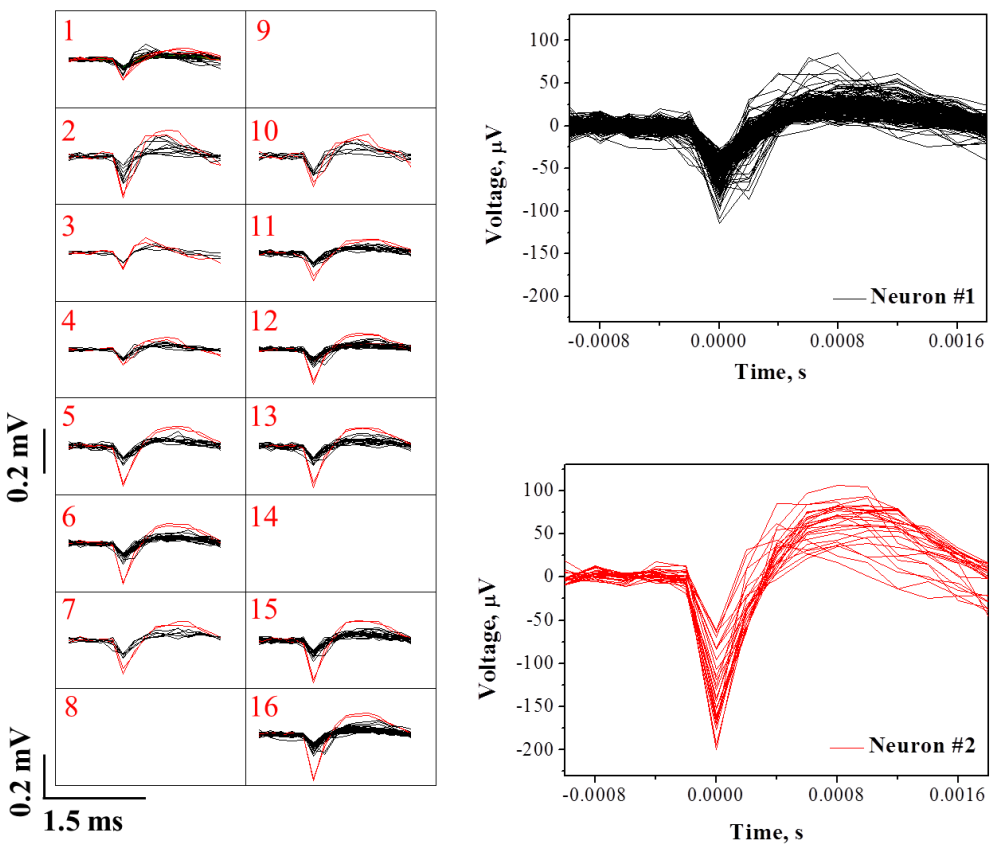

Figure 5-13. Spike sorting results of all MEA using the measured neural spike train signal.

Many researchers use correlation analysis to describe the relationship between measured neural spike signals [89, 91]. However, in this experiment is a problem in performing a correlation analysis of neural spike signals due to the amount of neural signal data was not sufficient to perform a correlation analysis. To perform a correlation analysis of neural spike signals measured on fabricated microprobe electrodes, it is necessary increase the number of microprobe electrodes. Future works will perform a correlation analysis using measured signals after adjusting the number of microprobe electrodes.

From the results of the *in-vitro* experiments, it was confirmed that the fabricated microprobe electrode successfully penetrated the dead cell layer of the hippocampal brain slice tissue and could measure the neural signal. In addition, the position of the inserted microprobe electrode was accurately confirmed through the transparent substrate.

5.4. Future works

The fabricated MEA successfully measured the neural signals of a cultured neuron and a hippocampal brain slice tissue. However, the amount of measured neural signal data is not sufficient to perform correlation analysis, it is necessary to adjust the number of electrodes for correlation analysis.

In addition, the fabricated MEA has a limitation for its utilization in other bio-applications. The microprobe structure fabricated in this study has the same height. At this time, the exposed portion of the electrode also has the same height. When the fabricated microprobe electrode is inserted into the tissue, the measured signal is a neural signal generated in the same layer.

This microprobe electrode has the limitation that signals from different layers of a multilayer structure (e.g., retinal tissue) [92] cannot be simultaneously measured, as shown in Figure 5-14. As it is important to measure and analyze the signals generated by each layer, microprobe electrode structures of different heights are required. The simultaneous measurement of neuron signals in each of the layers of the retina using a multi-height microprobe can be a useful application for analyzing the retina signals in detail. In addition, the fabricated MEA has structural limitations in signal measurement using nerve fibers. As the location of the axon varies in the nerve fiber, microprobe electrodes of various heights are required when measuring its signals [93]. Owing to these structural limitations, in the future work, it will be necessary to fabricate structures with different heights according to the target tissue.

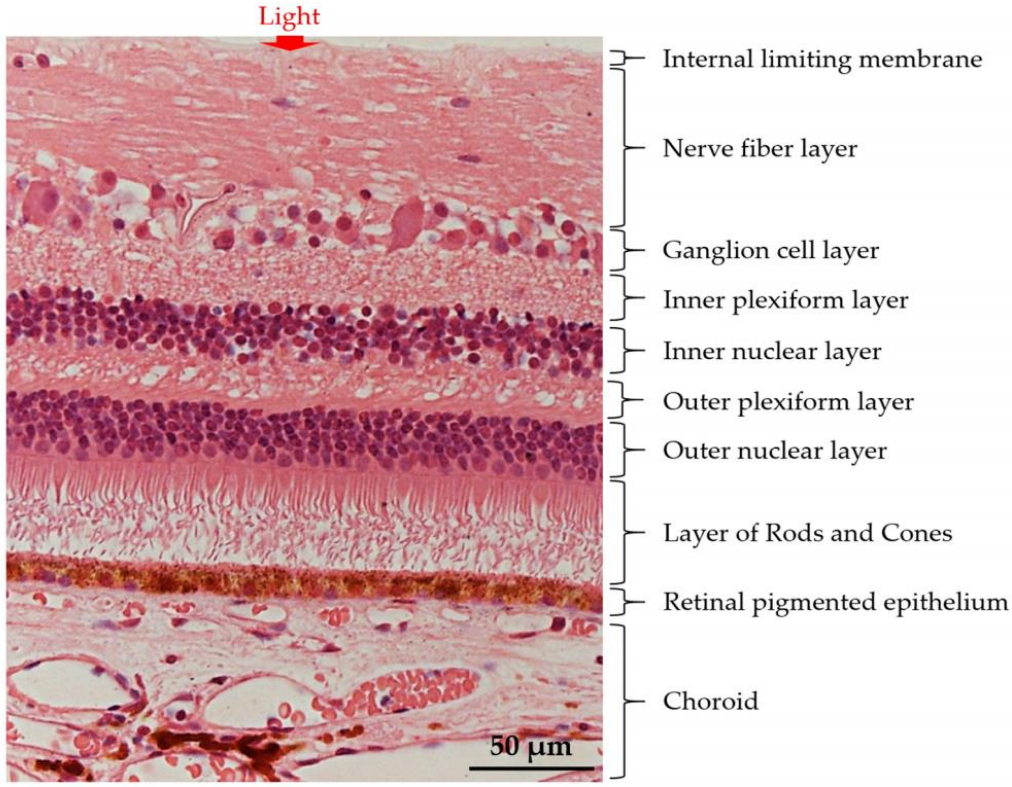

Figure 5-14. Basic retinal structure [92].

Chapter 6. Conclusion

In this study, a structure combining a silicon TGV electrode and an MEA has been proposed for a wide variety of biological applications, such as insertion in brain tissues for neural signal measurement. By using the silicon via electrode, the proposed structure can minimize the signal loss due to the addressing line, which is a problem in the conventional MEA structure. In addition, a problem of the conventional MEA is that owing to its opaque structure, the electrode cannot be inserted into the desired position and the target tissue may be damaged. To solve such a problem, a reflowed glass substrate having a transparency property is used, making it possible to accurately insert the microprobe electrode into the desired position and thereby minimizing the damage to the tissue.

The microprobe structure was fabricated using multi-DRIE and RIE processes. When fabricating the probe structure, we measured and analyzed the change in sharpness according to the depth of the first DRIE. The distance between the microprobe electrodes is designed to be 210 μm to prevent electrochemical crosstalk.

The TGV structure is manufactured by bonding silicon wafers and glass wafers using a low-vacuum anodic bonding process and then filling the gap between the silicon pillars with glass using a glass reflow process at 850 ℃. The resistance and coupling capacitance were measured to analyze the electrical characteristics of the fabricated TGV. The measurement results were 1.26 ± 0.041 Ω and 0.23 ± 0.03 pF, respectively. These measurements show that the resistance is low enough to measure neural signals and that the signal loss can be small owing to the small coupling capacitance between the silicon-via electrodes. To evaluate the

electrochemical properties of the combined structure of TGV and microprobe electrodes, EIS measurements were performed. The EIS measurements detect the change in impedance with frequency variation. The measurement results confirmed that the impedance of all the 16 electrodes at 1 kHz did not exceed 1 MΩ. Based on the measurement results, the component values of the equivalent circuit were successfully estimated using the Randles equivalent circuit model of the microprobe electrode and the Z-view modeling program. The transparency of the fabricated TGV structure was measured using a UV/Vis spectrophotometer. The measurement results showed a transparency of 60% or more in the visible region.

In-vitro experiments were conducted using the fabricated MEA structure. First, we observed that neural spike signals were successfully measured on 16 electrodes by culturing rat cortical neuron cells. After that, it was confirmed that the signals from three different neurons were measured. The average SNR of the measured signal is 14.4, which is higher than that of the conventional microprobe electrode. Finally, experiments using hippocampal brain slice tissue were performed. The experimental results showed that the microprobe electrode was successfully inserted into the hippocampal brain slice without damage, and the microprobe electrode inserted into the hippocampal brain slice tissue was accurately identified through the reflowed glass substrate. As a result of the signal measurement, it was confirmed that two different neuron signals were successfully measured. It was also confirmed that the microprobe electrode successfully measured the signal generated by the hippocampal neuron activity.

These results show that the proposed MEA can be used in various bio application areas as it overcomes the limitations of the conventional MEA structure.

Reference

[1] R. Caton, "Electrical Currents of the Brain," *The Journal of Nervous and Mental Disease*, vol. 2, pp. 610, 1875.

[2] D. Khudhair, S. Nahavandi, H. Garmestani, and A. Bhatti, "Microelectrode Arrays: Architecture, Challenges and Engineering Solutions," in *Emerging Trends in Neuro Engineering and Neural Computation*, A. Bhatti, K. H. Lee, H. Garmestani, and C. P. Lim, Eds. Singapore: Springer Singapore, pp. 41-59, 2017.

[3] H. J. Lee, Y. Son, J. Kim, C. J. Lee, E.-S. Yoon, and I.-J. Cho, "A multichannel neural probe with embedded microfluidic channels for simultaneous in vivo neural recording and drug delivery," *Lab on a Chip*, vol. 15, pp. 1590-1597, 2015.

[4] A. C. Patil, N. V. J. M. Thakor, B. Engineering, and Computing, "Implantable neurotechnologies: a review of micro- and nanoelectrodes for neural recording," *Medical & Biological Engineering & Computing*, journal article vol. 54, pp. 23-44, 2016.

[5] G. Xiao *et al.*, "A high-sensitive nano-modified biosensor for dynamic monitoring of glutamate and neural spike covariation from rat cortex to hippocampal sub-regions," *Journal of Neuroscience Methods*, vol. 291, pp. 122-130, 2017.

[6] E. Bloch, Y. Luo, and L. da Cruz, "Advances in retinal prosthesis systems," *Therapeutic Advances in Ophthalmology*, vol. 11, pp. 2515841418817501, 2019.

[7] V. K. Mushahwar, D. F. Collins, and A. Prochazka, "Spinal Cord

Microstimulation Generates Functional Limb Movements in Chronically Implanted Cats," *Experimental Neurology,* vol. 163, pp. 422-429, 2000.

[8] V. S. Polikov, P. A. Tresco, and W. M. Reichert, "Response of brain tissue to chronically implanted neural electrodes," *Journal of Neuroscience Methods,* vol. 148, pp. 1-18, 2005.

[9] H. Hubel David and N. Wiesel Torsten, "Ferrier lecture - Functional architecture of macaque monkey visual cortex," *Proceedings of the Royal Society of London. Series B. Biological Sciences,* vol. 198, pp. 1-59, 1977.

[10] D. A. Robinson, "The electrical properties of metal microelectrodes," *Proceedings of the IEEE,* vol. 56, pp. 1065-1071, 1968.

[11] M. E. Spira and A. Hai, "Multi-electrode array technologies for neuroscience and cardiology," *Nature Nanotechnology,* Review Article vol. 8, pp. 83, 2013.

[12] M. E. Spira, N. Shmoel, S.-H. M. Huang, and H. Erez, "Multisite Attenuated Intracellular Recordings by Extracellular Multielectrode Arrays, a Perspective," *Front. Neurosci.,* vol. 12, pp.212, 2018.

[13] A. Hai, J. Shappir, and M. E. Spira, "In-cell recordings by extracellular microelectrodes," *Nature Methods,* vol. 7, pp. 200, 2010.

[14] B. J. Black *et al.*, "Chronic recording and electrochemical performance of Utah microelectrode arrays implanted in rat motor cortex," *Journal of Neurophysiology,* vol. 120, pp. 2083-2090, 2018

[15] B. J. Kim *et al.*, "3D Parylene sheath neural probe for chronic recordings," *Journal of Neural Engineering,* vol. 10, p. 045002, 2013.

[16] J. G. Ha, Y. S. Song, S. H. Jung, Y. K. Kim, S. J. Bai, J. H. Park, and S. K.

Lee, "Novel microbial photobioelectrochemical cell using an invasive ultramicroelectrode array and a microfluidic chamber," *Biotechnology Letters,* vol. 39, pp. 849-855, 2017.

[17] R. Bhandari, S. Negi, L. Rieth, R. Normann, and F. Solzbacher, "A novel method of fabricating convoluted shaped electrode arrays for neural and retinal prostheses," *Sensors and Actuators A: Physical,* vol. 145, pp. 123-130, 2008.

[18] G. Ma and C. Wu, "Microneedle, bio-microneedle and bio-inspired microneedle: A review," *Journal of Controlled Release,* vol. 251, pp. 11-23, 2017.

[19] R. C. Gesteland, B. Howland, J. Y. Lettvin, and W. H. Pitts, "Comments on Microelectrodes," *Proceedings of the IRE,* vol. 47, pp. 1856-1862, 1959.

[20] G. E. Loeb, R. A. Peck, and J. Martyniuk, "Toward the ultimate metal microelectrode," *Journal of Neuroscience Methods,* vol. 63, pp. 175-183, 1995.

[21] L. A. Geddes and R. J. A. o. B. E. Roeder, "Criteria for the Selection of Materials for Implanted Electrodes," *Annals of biomedical engineering,* vol. 31, pp. 879-890, 2003.

[22] S. F. Cogan, "Neural Stimulation and Recording Electrodes," *Annu. Rev. Biomed. Eng.,* vol. 10, pp. 275-309, 2008.

[23] M. P. Ward, P. Rajdev, C. Ellison, and P. P. Irazoqui, "Toward a comparison of microelectrodes for acute and chronic recordings," *Brain Research,* vol. 1282, pp. 183-200, 2009.

[24] D. C. Bradley *et al.*, "Visuotopic Mapping Through a Multichannel

Stimulating Implant in Primate V1," *Journal of Neurophysiology,* vol. 93, pp. 1659-1670, 2005.

[25] S. Musallam, M. J. Bak, P. R. Troyk, and R. A. Andersen, "A floating metal microelectrode array for chronic implantation," *Journal of Neuroscience Methods,* vol. 160, pp. 122-127, 2007.

[26] A. Prasad *et al.*, "Comprehensive characterization and failure modes of tungsten microwire arrays in chronic neural implants," *Journal of Neural Engineering,* vol. 9, pp. 056015, 2012.

[27] B. Ghane-Motlagh, Sawan, Mohamad, "A review of Microelectrode Array technologies: Design and implementation challenges," *2013 2nd International Conference on Advances in Biomedical Engineering,* pp. 38-41, 2013.

[28] H. Scherberger *et al.*, "Magnetic resonance image-guided implantation of chronic recording electrodes in the macaque intraparietal sulcus," *Journal of Neuroscience Methods,* vol. 130, pp. 1-8, 2003.

[29] E. W. Keefer, B. R. Botterman, M. I. Romero, A. F. Rossi, and G. W. Gross, "Carbon nanotube coating improves neuronal recordings," *Nature Nanotechnology,* vol. 3, pp. 434, 2008.

[30] A. Prasad et al., "Abiotic-biotic characterization of Pt/Ir microelectrode arrays in chronic implant," *Front. Neuroeng.,* vol.7, pp.2, 2014.

[31] K. C. Cheung, "Implantable microscale neural interfaces," *Biomedical Microdevices,* vol. 9, pp. 923-938, 2007.

[32] J. R. N. J. W. Lathrop, "Semiconductor construction," *U. S. Patent No. 2,890,395,* 1959.

[33] K. D. Wise, J. B. Angell, and A. Starr, "An Integrated-Circuit Approach to Extracellular Microelectrodes," *IEEE Transactions on Biomedical Engineering,* vol. BME-17, pp. 238-247, 1970.

[34] K. D. Wise and J. B. Angell, "A microprobe with integrated amplifiers for neurophysiology," in *1971 IEEE International Solid-State Circuits Conference. Digest of Technical Papers*, vol. 14, pp. 100-101, 1971.

[35] J. Ji, K. Najafi, and K. D. Wise, "A scaled electronically-configurable multichannel recording array," *Sensors and Actuators A: Physical,* vol. 22, pp. 589-591, 1990.

[36] S. J. Tanghe and K. D. Wise, "A 16-channel CMOS neural stimulating array," *IEEE Journal of Solid-State Circuits,* vol. 27, pp. 1819-1825, 1992.

[37] J. Ji, K. Najafi, and K. D. Wise, "A low-noise demultiplexing system for active multichannel microelectrode arrays," *IEEE Transactions on Biomedical Engineering,* vol. 38, no. 1, pp. 75-81, 1991.

[38] K. Changhyun and K. D. Wise, "A 64-site multishank CMOS low-profile neural stimulating probe," *IEEE Journal of Solid-State Circuits,* vol. 31, pp. 1230-1238, 1996.

[39] K. D. Wise, D. J. Anderson, J. F. Hetke, D. R. Kipke, and K. Najafi, "Wireless implantable microsystems: high-density electronic interfaces to the nervous system," *Proceedings of the IEEE,* vol. 92, pp. 76-97, 2004.

[40] K. D. Wise, A. M. Sodagar, Y. Yao, M. N. Gulari, G. E. Perlin, and K. Najafi, "Microelectrodes, Microelectronics, and Implantable Neural Microsystems," *Proceedings of the IEEE,* vol. 96, pp. 1184-1202, 2008.

[41] M. R. Abidian and D. C. Martin, "Experimental and theoretical

characterization of implantable neural microelectrodes modified with conducting polymer nanotubes," *Biomaterials,* vol. 29, pp. 1273-1283, 2008..

[42] T. Gabay *et al.*, "Electro-chemical and biological properties of carbon nanotube based multi-electrode arrays," *Nanotechnology,* vol. 18, p. 035201, 2007.

[43] C. M. Lopez *et al.*, "An Implantable 455-Active-Electrode 52-Channel CMOS Neural Probe," *IEEE Journal of Solid-State Circuits,* vol. 49, pp. 248-261, 2014.

[44] M. E. J. Obien, K. Deligkaris, T. Bullmann, D. J. Bakkum, and U. Frey, "Revealing neuronal function through microelectrode array recordings," *Front. Neurosci.*, vol. 8, pp. 423, 2015.

[45] M. D. Gingerich, J. F. Hetke, D. J. Anderson, and K. D. Wise, "A 256-Site 3D CMOS Microelectrode Array for Multipoint Stimulation and Recording in the Central Nervous System," *Transducers '01 Eurosensors XV,* pp. 416-419, 2001.

[46] P. K. Campbell, K. E. Jones, R. J. Huber, K. W. Horch, and R. A. Normann, "A silicon-based, three-dimensional neural interface: manufacturing processes for an intracortical electrode array," *IEEE Transactions on Biomedical Engineering,* vol. 38, pp. 758-768, 1991.

[47] R. A. Normann, "Technology Insight: future neuroprosthetic therapies for disorders of the nervous system," *Nature Clinical Practice Neurology,* vol. 3, pp. 444, 2007.

[48] E. M. Maynard, C. T. Nordhausen, and R. A. Normann, "The Utah

Intracortical Electrode Array: A recording structure for potential brain-computer interfaces," *Electroencephalography and Clinical Neurophysiology,* vol. 102, pp. 228-239, 1997.

[49] S. F. Ronner and B. G. Lee, "Excitation of visual cortex neurons by local intracortical microstimulation," *Experimental Neurology,* vol. 81, pp. 376-395, 1983.

[50] R. A. Normann, E. M. Maynard, P. J. Rousche, and D. J. Warren, "A neural interface for a cortical vision prosthesis," *Vision Research,* vol. 39, pp. 2577-2587, 1999.

[51] B. Ghane Motlagh, M. Choueib, A. Hajhosseini Mesgar, M. Hasanuzzaman, and M. Sawan, "Direct Growth of Carbon Nanotubes on New High-Density 3D Pyramid-Shaped Microelectrode Arrays for Brain-Machine Interfaces," *Micromachines,* vol. 7, pp. 163, 2016.

[52] E. Fernández *et al.*, "Acute human brain responses to intracortical microelectrode arrays: challenges and future prospects," *Front. Neuroeng.*, vol. 7, pp. 24, 2014.

[53] T. D. Y. Kozai, A. S. Jaquins-Gerstl, A. L. Vazquez, A. C. Michael, and X. T. Cui, "Brain Tissue Responses to Neural Implants Impact Signal Sensitivity and Intervention Strategies," ACS Chemical Neuroscience, vol. 6, pp. 48-67, 2015.

[54] C. Spindt, C. Holland, A. Rosengreen, and I. Brodie, "Field-emitter arrays for vacuum microelectronics," *IEEE Transactions on Electron Devices,* vol. 38, pp. 2355-2363, 1991.

[55] J. Orloff and L. W. Swanson, "An asymmetric electrostatic lens for field-

emission microprobe applications," *Journal of Applied Physics*, vol. 50, pp. 2494-2501, 1979.

[56] Y. M. Shin, S. K. Lee, S. Jang, and J. H. Park, "Superhydrophobic properties of a hierarchical structure using a silicon micro-tip array decorated with ZnO nanowires," *Current Applied Physics*, vol. 14, pp. 665-671, 2014.

[57] E. Peiner, L. Doering, M. Balke, and A. J. M. T. Christ, "Silicon cantilever sensor for micro-/nanoscale dimension and force metrology," *Microsystem Technologies*, vol. 14, pp. 441-451, 2008.

[58] J. L. Amphlett, and G. Denuault, "Scanning Electrochemical Microscopy (SECM): An Investigation of the Effects of Tip Geometry on Amperometric Tip Response," *The Journal of Physical Chemistry B*, vol. 102, pp. 9946-9951, 1998.

[59] V. T. Binh, and J. Marien, "Characterization of microtips for scanning tunneling microscopy," *Surface science*, vol. 202, pp. 539-549, 1988.

[60] K. Najafi, and J. F. Hetke, "Strength characterization of silicon microprobes in neurophysiological tissues," *IEEE Transactions on Biomedical Engineering*, vol. 37, pp. 474-481, 1990.

[61] N. A. Aziz and B. Y. Majlis, "Fabrication study of solid microneedles array using HNA," *2006 IEEE International Conference on Semiconductor Electronics*, pp. 20-24, 2006,

[62] Y. Hanein, C. G. Schabmueller, G. Holman, P. Lücke, D. D. Denton, and K. F. Böhringer, "High-aspect ratio submicrometer needles for intracellular applications," *Journal of Micromechanics and Microengineering*, vol. 13,

pp. S91, 2003.

[63] H. Sasaki, M. Shikida, and K. Sato, "Fabrication of densely arrayed Si needles with large height for transdermal drug delivery system application," *IEEJ Transactions on Electrical and Electronic Engineering*, vol. 2, pp. 340-347, 2007.

[64] J. G. Ha, S. K. Lee, S. J. Bai, Y. K. Kim, and J. H. Park, "Conductive microtip electrode array with variable aspect ratio using combination process of reactive ion etching," *Journal of Micromechanics and Microengineering*, vol. 23, pp. 115009, 2013.

[65] Y. M. Shin, Y. K. Kim, S. K. Lee, and J. H. Park, "Single-mask fabrication of microprobe electrode array with various tip heights and sharpness using isotropic and anisotropic etching," *Micro and Nano Letters*, vol. 13, pp. 1245-1247, 2018.

[66] T. Wang, W. Yang, H. Huang, and C. Fu, "A novel fabrication method of flexible micro electrode array for neural recording," *2007 IEEE 20th International Conference on Micro Electro Mechanical Systems (MEMS)*, pp. 295-300, 2007.

[67] C. D. James *et al.*, "Extracellular recordings from patterned neuronal networks using planar microelectrode arrays," *IEEE Transactions on Biomedical Engineering*, vol. 51, pp. 1640-1648, 2004.

[68] W. Nisch, J. Böck, U. Egert, H. Hämmerle, and A. Mohr, "A thin film microelectrode array for monitoring extracellular neuronal activity in vitro," *Biosensors and Bioelectronics*, vol. 9, pp. 737-741, 1994.

[69] Y. M. Shin, Y. K. Kim, S. K. Lee, H. Shin, I. J. Cho, and J. H. Park,

"Microprobe electrode array with individual interconnects through substrate using silicon through-glass via," *Sensors and Actuators B: Chemical,* vol. 290, pp. 336-346, 2019.

[70] Y. M. Shin, Y. K. Kim, S. K. Lee, and J. H. Park, "Fabrication and measurements of an individually addressable microprobe electrode array using silicon through-glass via," in *2017 IEEE 30th International Conference on Micro Electro Mechanical Systems (MEMS)*, pp. 648-651, 2017.

[71] Y. T. Lee, S. R. Yeh, Y. C. Chang, and W. Fang, "Integration of silicon-via electrodes with different recording characteristics on a glass microprobe using a glass reflowing process," *Biosensors and Bioelectronics,* vol. 26, pp. 4739-4746, 2011.

[72] C. W. Chang *et al.*, "A double-sided, single-chip integration scheme using through-silicon-via for neural sensing applications," *Biomedical Microdevices,* vol. 17, pp. 11, 2015.

[73] B. E. Volland, H. Heerlein, I. Kostic, and I. W. Rangelow, "The application of secondary effects in high aspect ratio dry etching for the fabrication of MEMS," *Microelectronic Engineering,* vol. 57-58, pp. 641-650, 2001.

[74] S. Yoo, C. H. Ji, J. Y. Jin, and Y. K. Kim, "Suppression of surface crystallization on borosilicate glass using RF plasma treatment," *Applied Surface Science,* vol. 316, pp. 484-490, 2014.

[75] S. B. Goncalves, J. F. Ribeiro, A. F. Silva, R. M. Costa, and J. H. Correia, "Design and manufacturing challenges of optogenetic neural interfaces: a review," *Journal of Neural Engineering,* vol. 14, pp. 041001, 2017.

[76] K. Leonhardt *et al.*, "Atomic Force Microscopy-Scanning Electrochemical Microscopy: Influence of Tip Geometry and Insulation Defects on Diffusion Controlled Currents at Conical Electrodes," *Analytical Chemistry,* vol. 83, pp. 2971-2977, 2011.

[77] X. Qian, N. Gu, Z. Cheng, X. Yang, E. Wang, and S. Dong, "Impedance study of (PEO)10LiClO4–Al2O3 composite polymer electrolyte with blocking electrodes," *Electrochimica Acta,* vol. 46, pp. 1829-1836, 2001.

[78] P. Xiao, D. Liu, B. B. Garcia, S. Sepehri, Y. Zhang, and G. Cao, "Electrochemical and photoelectrical properties of titania nanotube arrays annealed in different gases," *Sensors and Actuators B: Chemical,* vol. 134, pp. 367-372, 2008.

[79] P. Yu and G. S. Wilson, "An independently addressable microbiosensor array: What are the limits of sensing element density?," *Faraday Discussions,* vol. 116, pp. 305-317, 2000.

[80] C. M. Au - Hales, J. D. Au - Rolston, and S. M. Au - Potter, "How to Culture, Record and Stimulate Neuronal Networks on Micro-electrode Arrays (MEAs)," *JoVE,* vol. 39, p. e2056, 2010.

[81] G. Hong *et al.*, "A method for single-neuron chronic recording from the retina in awake mice," *Science,* vol. 360, p. 1447, 2018.

[82] A. Canales *et al.*, "Multifunctional fibers for simultaneous optical, electrical and chemical interrogation of neural circuits in vivo," *Nature Biotechnology,* vol. 33, p. 277, 2015.

[83] T. Saxena *et al.*, "The impact of chronic blood–brain barrier breach on intracortical electrode function," *Biomaterials,* vol. 34, pp. 4703-4713,

2013.

[84] C. Lin, C. Chang, Y. Lee, R. Chen, Y. Chang, and W. Fang, "Glass Microprobe with Embedded Silicon Vias for 3D Integration," *2009 IEEE 22nd International Conference on Micro Electro Mechanical Systems*, pp. 200-203, 2009.

[85] S. Suner, M. R. Fellows, C. Vargas-Irwin, G. K. Nakata, and J. P. Donoghue, "Reliability of signals from a chronically implanted, silicon-based electrode array in non-human primate primary motor cortex," *IEEE Transactions on Neural Systems and Rehabilitation Engineering*, vol. 13, pp. 524-541, 2005.

[86] C. H. Chen *et al.*, "A three-dimensional flexible microprobe array for neural recording assembled through electrostatic actuation," *Lab on a Chip*, vol. 11, pp. 1647-1655, 2011.

[87] K. Reinhard *et al.*, "Step-By-Step Instructions for Retina Recordings with Perforated Multi Electrode Arrays," *PLOS ONE*, vol. 9, p. e106148, 2014.

[88] R. Fiáth *et al.*, "A silicon-based neural probe with densely-packed low-impedance titanium nitride microelectrodes for ultrahigh-resolution in vivo recordings," *Biosensors and Bioelectronics*, vol. 106, pp. 86-92, 2018.

[89] J. P. J. Savarraj, and A. W. L. Chiu, "Network Dynamics and Spontaneous Oscillations in a Developing Neuronal Culture," *American Journal of Biomedical Engineering*, vol. 4, pp. 17-24, 2014.

[90] P. J. Lein, C. D. Barnhart, and I. N. Pessah, "Acute Hippocampal Slice Preparation and Hippocampal Slice Cultures," in *In Vitro Neurotoxicology: Methods and Protocols*, L. G. Costa, G. Giordano, and M. Guizzetti, Eds.

Totowa, NJ: Humana Press, pp. 115-134, 2011,

[91] J. Fournier, C. M. Mueller, M. Shein-Idelson, M. Hemberger, and G. Laurent, "Consensus-Based Sorting of Neuronal Spike Waveforms," *PLOS ONE*, vol. 11, pp. e0160494, 2016.

[92] S. L. S. Ding, S. Kumar, and P. Mok, "*Cellular Reparative Mechanisms of Mesenchymal Stem Cells for Retinal Diseases*," *Int. J. Mol. Sci.*, vol.18, p. 1406, 2017.

[93] R. A. Normann and E. Fernandez, "Clinical applications of penetrating neural interfaces and Utah Electrode Array technologies," *Journal of Neural Engineering*, vol. 13, p. 061003.

국문초록

본 논문은 투명한 특성을 갖는 유리 기판 관통 실리콘 비아를 사용하여 개별 상호 연결을 갖는 수직 평면 외 마이크로 전극 어레이의 개발에 대한 것이다. 이러한 마이크로 프로브 전극 어레이는 뇌 조직에 삽입하여 신경 신호 측정을 위한 다양한 생물학적 응용에서 사용될 수 있다. 기존에 연구된 마이크로 프로브 전극 어레이는 불투명한 전극 구조의 삽입에 의해 원치 않는 조직 손상과 어드레싱 라인에서 발생하는 신호 손실이 문제가 된다. 이러한 문제를 해결하기 위해 저저항 실리콘 웨이퍼와 유리 재흘림 공정을 이용하여 유리 기판 관통 실리콘 비아와 마이크로 프로브 전극을 제작하는 것을 목표로 한다. 유리 재흘림 공정으로 제작되는 유리기판은 투명한 성질을 가지므로 마이크로 프로브 전극을 원하는 위치에 삽입함으로써 조직의 손상을 최소화할 수 있다. 또한, 제작되는 유리기판은 절연막으로서 우수한 특성을 가지기 때문에 실리콘 비아 전극 간의 신호 손실을 최소화할 수 있다.

유리 기판 관통 실리콘 비아 구조의 직경 및 높이는 각각 80 μm 와 250 μm가 되도록 설계되었다. 먼저 DRIE 공정을 이용하여 직경 80 μm 실리콘 기둥을 제작한 후 붕규산 유리 웨이퍼를 실리콘 웨이퍼에 접착한 후 850 ℃의 온도에서 재흘림 공정을 수행하여 제작된다. 제작이 완료된 유리 기판 관통 실리콘 비아 구조의 투명도는 UV/Vis 분광 광도계를 사용하여 측정되었다. 측정 결과 가시광 영역에서 60 % 이상의 투명성을 가지는 것을 확인하였다. 제작된 싱글 실리콘 비아의 저항은 1.26 ± 0.041 Ω으로 측정되었고 교차 결합 커패시턴스는 0.23 ± 0.03 pF로 측정되었다.

마이크로 프로브의 높이는 조직에 삽입하기 위해 90 μm 이상으로 설계되었으며 마이크로 프로브 사이의 간격은 전극 간의 화학적 누화를 최소화하기 위해 210 μm로 설계되었다. 마이크로 프로브 구조는 한번의

포토 리소그래피 공정과 단일 식각 마스크를 사용하여 DRIE 와 RIE과정을 결합한 공정을 수행하여 형성된다. 마이크로 프로브의 형상은 RIE 공정 동안 실리콘 마이크로 기둥 측벽의 위치 및 첫 번째 DRIE 공정의 깊이에 따른 식각 속도의 차이에 의해 얻을 수 있다.

마이크로 프로브를 개별전극으로 제작하기 위해 네거티브 포토레지스트 (DNR-L-300)을 사용하여 마이크로 프로브 구조를 노출하고 각각 200 Å 및 2000 Å의 Cr 및 Au 전도층을 증착하였다. 리프트 오프 공정을 이용하여 전극 패터닝 후 3000 Å 의 파릴렌-C 층을 절연막으로서 전극 상에 증착하였다. 그 후, 두꺼운 포토레지스트를 이용한 마스크가 필요 없는 자기 정렬 공정을 수행하여 마이크로 프로브 말단에만 도전층을 노출 시켜 개별 마이크로 프로브 전극 공정을 완료한다. 제작이 완료된 마이크로 프로브 전극은 개별적으로 유리 기판 관통 실리콘 비아를 통해 기판의 뒷면으로 직접 연결이 되는 구조이다.

개별 연결을 갖는 마이크로 프로브 전극의 전기화학적 특성을 확인하기 위해 각각의 전극의 정상 상태 제한 전류를 측정할 수 있는 순환 전압 전류법이 수행되었다. 그리고 측정 된 정상 상태 제한 전류는 이론값과 비교되었다. 또한 16개 전극에 대한 임피던스 측정이 수행되었으며 1 kHz에서의 평균 임피던스는 0.292 ± 0.156 MΩ으로 측정되었다. 그런 다음 측정된 데이터와 임피던스 모델링 소프트웨어 (Zview, AMETEK Scientific instruments)를 사용하여 마이크로 프로브 전극의 등가 회로 분석을 수행하였다.

그후 제작된 마이크로 프로브 전극에서 1차 쥐 대뇌 피질 뉴런 세포 (DIV 7)를 배양하고 신경 신호를 성공적으로 측정하였다. 측정된 신호의 평균 신호 대 잡음비는 14.4로 측정되었다. 또한 제작된 전극을 쥐의 해마 뇌 절편 조직에 삽입하고 실험을 수행하였다. 실험 결과 제조된 마이크로 프로브 전극은 높은 투명성으로 인해 프로브 전극을 해마

조직상의 원하는 위치에 삽입함으로써 조직 손상을 최소화 하며 신호를 성공적으로 측정할 수 있었다.

결론적으로 제안된 유리기판 관통 실리콘 비아와 개별적으로 연결된 마이크로 프로브 구조는 신호 대 잡음 비가 높고 화학적 누화가 없는 신호를 측정할 수 있으며 투명도가 높은 유리 기판 관통 실리콘 비아 구조를 사용하여 원하는 위치에 프로브 전극을 삽입하여 타겟 조직의 손상을 최소화할 수 있는 것을 확인하였다. 제안된 마이크로 프로브 전극은 기존의 전극 구조의 한계를 극복할 수 있기 때문에 좀 더 다양한 바이오 응용 분야에 적합하다고 할 수 있다.

감사의 글

5년간의 박사과정 논문을 마무리하며 많은 분께 감사를 드리고 싶어 감사의 글을 적습니다. 먼저 학위 기간 동안 때로는 자상하게 때로는 엄격하게 연구의 방향을 잡아주신 김용권 교수님께 감사드립니다. 또한 저의 부족한 박사학위 심사를 해주신 전국진 교수님, 박재형 교수님, 서종모 교수님, 김성재 교수님께 감사드립니다. 특히 박사 예비심사 후에 서종모 교수님께서 해주신 조언 및 제작된 소자를 이용한 바이오 실험에 대하여 도움을 주신 것에 다시 한번 감사드립니다. 그리고 단국대 이승기 교수님, 박재형 교수님께도 감사를 드리고 싶습니다. 대학원 생활을 시작한 2012년부터 2019년까지 부족한 저에게 연구에 대하여 자상하게 방향을 잡아주시고 지도를 해주셔서 감사드립니다. 그리고 박사학위 마지막에 바이오 실험을 흔쾌히 도와주신 조일주 박사님, 전상범 교수님께도 감사드립니다.

또한 지난 5년간 매일 같이 연구실 생활을 했던 선, 후배님들께 감사를 드립니다. 무엇보다 처음 석사 때 같이 과제를 진행하며 공정을 알려주며 저의 연구에 많은 도움을 준 준근이형에게 감사를 드리고 싶습니다. 또한 연구에 대하여 조언을 해주신 은석이형, 율이형, 승현이형, 정기, 영태형, 성현이형에게 감사를 드리고 싶습니다.

그리고 같이 대학원 생활을 했던 재성이형, 승택이형, 현석이형, 성환이형, 민혜, 석원이, 대곤이, 홍균이 민수, 용승이, 기홍이형, 그리고 석사부터 박사까지 대학원 생활을 같이 했던 이미 사회인이 된 성우와 함께 학위 수여의 기쁨을 나누고 싶습니다.

저의 박사학위 심사를 응원해준 현재 연구실 인원들에게 감사를 드리고 싶습니다. 다음 박사 졸업생이 될 명진이와 대호에게 앞으로 하는 연구가 잘 진행되기를 기원합니다. 이제 박사과정을 시작하는

경택이에게도 큰 슬럼프 없이 연구가 잘 진행되기를 기도합니다. 석사 졸업 후 해외 박사 유학을 가는 새영이에게도 해외 가서도 연구가 무탈하게 잘 진행되어 좋은 결과가 많이 나오길 기원합니다.

대학원 생활 동안 많은 응원을 해줬던 친구들에게도 고맙다는 말을 전하고 싶습니다. 서로 대학원 생활을 하며 주말마다 응원을 해주고 박사 심사 통과 후 누구보다 축하를 해줬던 정호에게 고맙다는 말을 전하고 싶습니다. 또한 지금까지 연락을 주고받으며 응원을 해준 고등학교 친구들 강훈이, 명수, 선현이, 범균이, 준범이, 용석이, 한우, 현우에게도 감사의 말을 전합니다. 의정부에서 항상 응원을 해줬던 초등학교 친구들인 김현준, 윤현준 두 현준에게도 고맙다는 말을 전하고 싶습니다.

그리고 무엇보다 대학원 생활 동안 많은 고생을 하신 부모님께 감사드립니다. 묵묵히 뒤에서 지켜봐 주시며 응원해 주셨던 아버지, 어머니께 다시 한번 감사드립니다. 이제부터는 학생이 아닌 사회인으로써 부모님께 효도하도록 하겠습니다. 그리고 항상 힘들 때마다 응원해줬던 누나, 성민이형에게도 감사드립니다. 그리고 항상 앞에서 재롱을 부리며 웃음을 주었던 조카들 은빈이, 지우에게도 더 좋은 삼촌이 되도록 노력하겠습니다.

이제 학생이 아닌 사회인으로 다시 새 출발을 시작하려고 하니 아쉬움과 기쁨이 교차하는 것 같습니다. 어딜 가든 성실하게 주어진 일에 최선을 다하겠다는 마음 가짐으로 살겠다고 스스로 다짐하며 감사의 글을 마칩니다.